The drone latency location routing problem under uncertainty

Transportation Research Part C 156 (2023) 104322

Contents lists available at ScienceDirect

Transportation Research Part C

journal homepage: www.elsevier.com/locate/trc

The drone latency location routing problem under uncertainty

Maria Elena Bruni [a,c,*], Sara Khodaparasti [b], Guido Perboli [b,c]

[a] Department of Mechanical, Energy and Management Engineering, University of Calabria, Rende, Cosenza, Italy
[b] Department of Management and Production Engineering, Polytechnic University of Turin, Turin, Italy
[c] CIRRELT, Montreal, Canada

ARTICLE INFO

Keywords:
Drone delivery
Latency
Fulfillment center selection
Robust optimization
Branch & Check

ABSTRACT

This paper addresses a location routing problem arising in the last-mile drone delivery context, where drones are used to deliver small packages to a set of customers. Each drone is launched from a fulfillment center to serve multiple customers on a single trip. The goal is to find the optimal subset of fulfillment centers to use as drone launching and landing platforms and the optimal drone routes with the aim of minimizing the sum of customers' waiting times. We study the problem under two realistic assumptions. First, the drone energy consumption is a nonlinear function of the drone load that varies along the route, as parcels are delivered. Second, the drone flight time is not deterministically known. To hedge against drone flight time uncertainty, we adopt a robust optimization approach. Due to the complex nature of the problem, which turns out to be a nonlinear mixed-integer problem, we design an exact method based on a tailored efficient Branch & Check algorithm that uses customized no-good cuts. The computational experiments show the validity of the proposed model and the promising performance of the exact method. Moreover, we present a case study on last-mile parcel delivery in Turin, Italy, providing insights into the advantages of a drone-based delivery system.

1. Introduction

The disruptive impact of e-commerce on city logistics has posed significant challenges for transportation companies (Perboli and Rosano, 2019; Perboli et al., 2021a). This impact is not only due to the increased volume of small, frequent last-mile deliveries, often characterized by tight time-windows, but also to the changing behavior of customers who are becoming more connected and informed. In order to develop effective solutions, it is essential to rethink city logistics with a customer-centric focus, adapting to the evolving needs.

As a result, traditional cost-based models are being threatened, and companies are exploring new delivery methods (Crainic et al., 2021; Perboli et al., 2018b) as drones, that have the potential to disrupt last-mile delivery (McKinsey, 2023). Forward-thinking companies are already planning for a future where drones will play a significant role, conducting proofs-of-concept to test their feasibility in the context of city logistics. Examples include "Amazon Prime Air" introduced in late 2013 (Bensinger, 2013), Google's Wing (Kanellos, 2014; Verge, 2023), which has made 300,000 commercial drone deliveries in the U.S., Europe, and Australia, and Walmart and its partners (such as Zipline (2023)), which completed 6000 deliveries in the United States last year.

Drones may streamline last-mile operations in different ways, leading to considerable cost savings (since they have lower operational and maintenance costs, compared to terrestrial vehicles), and delivery time reduction; notably, they are eco-friendly (Goodchild and Toy, 2018) and almost noise- and traffic-free, all characteristics in line with emerging green and sustainable logistics

* Corresponding author at: Department of Mechanical, Energy and Management Engineering, University of Calabria, Rende, Cosenza, Italy.
E-mail addresses: mariaelena.bruni@unical.it (M.E. Bruni), sara.khodaparasti@unical.it (S. Khodaparasti), guido.perboli@polito.it (G. Perboli).

https://doi.org/10.1016/j.trc.2023.104322
Received 21 February 2023; Received in revised form 29 August 2023; Accepted 30 August 2023
Available online 15 September 2023

goals (Melkonyan et al., 2020). In addition, drones often represent the unique option to reach distant and/or isolated areas. For these reasons, drones are increasingly used in a wide range of applications, such as surveillance (Panadero et al., 2020; Di Puglia Pugliese et al., 2021), humanitarian logistics (Zhang and Li, 2023; Kyriakakis et al., 2022; Ghelichi et al., 2021), and traffic monitoring (Barmpounakis and Geroliminis, 2020).

Despite these advantages, the integration of drones into city logistics poses operational challenges and has limitations (Benarbia and Kyamakya, 2022) among which limited payload capacity and flight range (Moshref-Javadi and Winkenbach, 2021). For this reason, drone logistics has been usually considered in a collaborative framework, where traditional vehicles support drone operations. Since this solution brings non-trivial synchronization issues between vehicles and drones, more often, logistics facilities as Fulfillment Centers (FCs) are used to support drone delivery services. In particular, in FCs, drones can be launched and retrieved, reloaded and recharged. This poses the problem of the optimal selection of FCs, since a wrong choice could hinder the efficiency of the service, increasing power consumption, flight distance, and total customers' waiting time.

It is worth noting that while the recent literature has extensively studied truck and drone delivery systems, location routing problems with drones have received relatively less attention. This problem combines two sub-problems: the FCs selection problem and the latency routing problem, where the objective is the minimization of the customers' waiting time, also called latency. The very few scientific contributions that tackled the two problems (location and routing) in an integrated model neglect two fundamental characteristics of drones, namely the limited payload and the energy consumption model. While the former is relatively straightforward, the latter plays a critical role in determining the performance of drone delivery systems, especially when multiple visits are allowed in a single drone trip. The majority of the models in the drone-aided literature incorporate energy consumption only indirectly through flight time limits or flight distance limits. In the best-case scenario, where the fundamental physical forces involved in flight are approximated, energy consumption is modeled as a linear function of flight time (Troudi et al., 2018; Dorling et al., 2016), which is a crucial factor affecting battery consumption (Zhang et al., 2021). In this paper, following the approach proposed by Dorling et al. (2016) and then used in Cheng et al. (2020a), we explicitly consider the internal and external factors that affect energy consumption, namely the drone design (like the weight of different drone parts, the number of rotors), the environment (like air density, gravitational force), and the load carried out by the drone. This last aspect adds complexity to the problem for two reasons. First, the load carried out by drones depends on the assignment of customers to drones. Second, the load of the drone varies each time a package is delivered, and hence, it is directly influenced by the routing plan to be optimized. Ignoring load-dependent energy consumption can lead to an underestimation of the energy consumption. Additionally, we indirectly incorporate the effects of wind speed, weather conditions, and physical obstacles like the canyons of tall buildings (Vural et al., 2021a; Evers et al., 2014) by considering flight time uncertain. In fact, the exogenous uncertain factors mentioned above have a direct impact on the drone speed, and hence, on the flight time. The incorporation of the uncertainty in flight time strongly affects the total customers' waiting time, which is the key customer-centric Key Performance Indicator (KPI) that we want to optimize. Recently, the issue of incorporating uncertainty into latency-based routing problems has been addressed in Beraldi et al. (2019), Bruni et al. (2020a,b) and Bruni et al. (2018).

Summarizing, the contributions of this paper are as follows. We introduce the Drone Latency Location Routing Problem (DLLRP) as a new problem able to jointly address the FCs selection and the drone routing problem, considering load-dependent drone energy requirements. The problem is addressed within a robust optimization framework (Ben-Tal and Nemirovski, 2002), where uncertainty affects the energy consumption constraints through uncertain flight times. Rather originally, we consider a nonlinear robust optimization model, for which we derive deterministic counterparts for two commonly used uncertainty sets. The resulting problem is a robust optimization problem, where robust constraints are nonlinear in the decision variables even when linear uncertainty sets are considered. Only a few papers have addressed nonlinear robust optimization models (see for instance Yuan et al. (2018), Mittal et al. (2011) and Kolvenbach et al. (2018)): this is the only paper in the routing context and one of the very few presenting an exact solution approach. Previous work by the same authors (Bruni and Khodaparasti, 2022) addressed a simplified version of the model with a box uncertainty set and presented a heuristic approach. In this paper, we extend the research providing an efficient exact algorithm to address the computational complexity of the problem, also considering the more complex case of ellipsoidal uncertainty, which is deemed more appropriate for flight time uncertainty (Chassein et al., 2019) and is less conservative than the box case. To the best of our knowledge, this is the first location routing model for drone delivery that simultaneously accounts for all these aspects.

The rest of this paper is organized as follows. Section 2 discusses the related literature. Section 3 presents the problem and a discussion on drone energy consumption under uncertain flight times. The deterministic counterparts are then derived for two uncertainty sets. Section 4 describes the exact solution approach. Section 5 is devoted to an extensive computational study carried out with the aim of assessing the performance of the exact method. Section 6 provides managerial insights through a case study, concerning the metropolitan area of Turin (Italy), derived from recent collaborations of the authors with the Center for Automotive Research and Sustainable mobility of Politecnico di Torino (CARS@Polito) and the Regional Government of Piedmont, as part of the development of the new Logistics and Mobility Plan to be implemented in 2025 (CARS@POLITO, 2012; Perboli et al., 2021a,b). Finally, Section 7 concludes the paper.

2. Literature review

Over the last decade, abundant research has been conducted concerning drone-aided delivery systems (the reader is referred to the recent surveys (Moshref-Javadi and Winkenbach, 2021; Macrina et al., 2020; Poikonen and Campbell, 2021)). The multi-depot drone delivery problem (also with facility location) has recently received some attention. Table 1 classifies such contributions

Table 1
Characteristics of the contributions on multi-depot/location problems.

	Location	*Routing*	*Drone payload*	*Energy consumption*
Yakıcı (2016)	*I*	✓	✗	✗
Chowdhury et al. (2017)	–	✗	✓	Linear
Golabi et al. (2017)	–	✗	✓	✗
Kim et al. (2017)	*H*	✓	✓	✗
Pulver and Wei (2018)	–	✗	✗	✗
Chauhan et al. (2019)	–	✗	✓	Linear
Liu et al. (2019)	*I*	✓	✗	✗
Macias et al. (2020)	*I*	✓	✗	Linear
Torabbeigi et al. (2020)	*H*	✓	✓	Linear
Kim et al. (2021)	*I*	✓	✓	✗
Li et al. (2021)	*I*	✓	✗	✗
Grogan et al. (2021)	*I*	✓	✗	✗
Dukkanci et al. (2021)	–	✗	✓	Nonlinear (speed)
Vural et al. (2021a)	*I*	✓	✗	✗
Zhu et al. (2022)	*I*	✗	✓	Linear
This paper	*I*	✓	✓	Nonlinear

H: Hierarchical *I*: Integrated.

on the basis of the way the *Location* problem is addressed (either in a hierarchical or integrated model) and the presence or absence of *Routing* decisions. Other critical features such as *Drone payload* and *Energy consumption* constraints are also examined. We highlight that the distinguishing feature of drone routing problems, with respect to classical vehicle routing problems, is that energy consumption is not anymore a trivial function of flight time and speed, but also depends on the payload.

Yakıcı (2016) proposed a selective location routing model, with an upper bound on the number of selected stations to be used, where the importance value corresponding to the covered points is maximized. An ant colony optimization metaheuristic is designed to solve the problem. Chowdhury et al. (2017) and Golabi et al. (2017), in the humanitarian logistic context, proposed location models where drones assist people in affected areas. Kim et al. (2017) proposed a set covering model to find the optimal number of locations used as depots in a healthcare context, followed by a multi-depot drone routing model. A Lagrangian relaxation method was also proposed to solve the model. Pulver and Wei (2018) presented a bi-objective covering location model to find the optimal locations of drone launch sites for an emergency medical service application. Chauhan et al. (2019) studied the maximum coverage facility location problem with drones, where facilities act as launching sites for drones, performing back-and-forth trips. Liu et al. (2019) presented a model to find the optimal location of sites to launch the drones and the optimal drone routes minimizing the total cost, including base establishment cost, drone usage cost, and flight cost. Again, in the humanitarian relief context, Macias et al. (2020) proposed a combined location routing and trajectory model for locating uncapacitated hubs and optimizing drone trajectories in a relief distribution context. A trajectory optimization problem is used to optimize the state of charge in the drone battery at the end of the flight. Torabbeigi et al. (2020) proposed two mathematical formulations involving strategic and operational plans to optimize drone parcel delivery. At the strategic level, a set covering model is solved to determine the minimum number of depots to open such that all customers are covered; next, at the operational stage, a drone routing model is solved in order to find the minimum number of drones to dispatch from the open depots and the corresponding optimal paths. The authors included energy consumption constraints into the problem and modeled them as linear functions in terms of load and flight time. Kim et al. (2021) proposed a drone routing model with multiple depots, multiple drones, and flight range constraints. The objective function minimizes the routing cost and the cost assigned to drone usage. Li et al. (2021) studied a multi-depot drone routing problem to minimize the total number of drones used and the total traveled distance. The model accounts for a maximum drone flight time. To solve the problem, the authors developed a heuristic approach based on a hybrid large neighborhood search. In a recent paper, Grogan et al. (2021) proposed a multi-depot routing problem with application in relief operations conducted after a tornado. It is worthwhile noting that only a few studies in the location routing context have explicitly considered the energy consumption model. For the sake of completeness, we mention that Dukkanci et al. (2021) introduced an explicit calculation of the energy consumption as a nonlinear function of the drone speed in a problem where drones are transported by traditional vehicles (trucks).

Focusing on the contributions under uncertainty, Vural et al. (2021b) proposed a two-stage stochastic programming model to address the airbase location decisions and the drone routing plans simultaneously. The first stage decisions include the base location and the drone assignments to the bases. Drone routing plans represent the recourse decisions that are taken after knowing the weather realization. The model does not explicitly account for the energy consumption but a limit for the maximum drone flight time is considered. Zhu et al. (2022) presented a two-stage robust facility location problem, where drones are only allowed to perform back-and-forth trips. Considering a single-depot setting, Kim et al. (2018) studied drone flight scheduling under uncertainty on battery duration, expressed in terms of maximum flight time. The objective function is the minimization of the drone operating costs, used as a proxy for the number of drones. Flight duration is modeled as a robust parameter and the equivalent robust formulation is derived for the linear battery capacity constraint. Ulmer and Thomas (2018) considered uncertainty in customers' orders and studied a dynamic vehicle routing problem where drones and vehicles work separately to maximize the expected reward gained from delivering the orders within a deadline. Radzki et al. (2021a) addressed the drone routing problem under uncertainty of travel parameters, modeled as fuzzy numbers, as an extension to the deterministic model presented in Thibbotuwawa et al.

(2020). The model is solved for instances of up to 12 customers. In a recent study, Di Puglia Pugliese et al. (2021) adopted a robust optimization approach to address weather-related uncertainty in energy consumption for a synchronized truck and drone-based problem. In this problem, drones work in tandem with trucks to serve one customer for each trip. The proposed formulation minimizes transportation costs while drone and truck capacity, time windows and energy consumption are taken into account. The uncertain energy consumption is described as a piece-wise linear function, which depends on the period of time and is formulated for the budgeted polytope case. Instances of up to 15 customers are solved by a decomposition solution approach based on Benders' combinatorial cuts. A similar problem was addressed in Radzki et al. (2021b) with an approach based on constraint programming. The goal is to find feasible routes for a fleet of drones under changing weather conditions, guaranteeing a minimum level of customers' satisfaction, expressed as a percentage of the expected amount of goods delivered to the recipients. Zhang et al. (2023) presented a robust drone arc routing problem on a multi-graph. Lagrangian relaxation and branch-and-price framework are used to solve the problem. Flight duration is used to approximate the energy consumption of drones. Cheng et al. (2020b) considered the risk of drone delivery systems under uncertain wind conditions via the minimization of the essential riskiness index, to help meet delivery deadlines by limiting the probability of tardiness. The author assumes that drones have sufficient energy to perform a round trip and that wind conditions do not affect energy consumption.

The present study is different from the extant literature since it explicitly addresses the non-linear and uncertain nature of the energy consumption function. Moreover, it considers latency as the primary objective to be minimized in a location routing problem. None of the above mentioned papers has considered these issues before.

3. Problem description and mathematical formulation

The DLLRP is a location routing problem that determines the subset of launch and landing FCs for a fleet of drones with the aim of minimizing the customers' waiting time.

The problem assumptions are summarized as follows:

- The number of FCs is limited and each FC can host a pre-specified number of drones.
- The launching FC can be different from the retrieving FC.
- Drones are homogeneous in terms of maximum payload and battery capacity.
- Each drone can serve more than one customer on a trip.
- Battery consumption nonlinearly depends on the drone load, which varies as the parcels are dropped.
- Flight times are not deterministically known and this uncertainty affects both the arrival time at customers and the battery energy consumption.

Fig. 1 displays a solution of the DLLRP with three FCs, two drones, and nine customers.

In what follows, we present the deterministic formulation of the DLLRP, built upon the layered formulation (Nucamendi-Guillén et al., 2022; Bruni and Khodaparasti, 2022), which has been efficiently used to model latency-based objective functions (Bruni et al., 2020c,d,e). Fig. 2 describes a network stratified in levels or layers, and for this reason called multi-layer (Nucamendi-Guillén et al., 2016). The multi-layer network is built by adding the copies of n customers (depicted by a square) in each level and the copies of m potential FCs (depicted by a circle). The number of levels in the multi-layer network is denoted by N and depends on the number of customers to be serviced (n) and the number of drones available (k) (The number of levels is limited above $N = n - k + 1$. In fact, if $k-1$ drones just visit one customer, then the kth drone visits the remaining $n-(k-1)$ customers. Each level number (from 1 to N) represents the backward order of visits of a customer: the last customer is in Level 1, the last but one in Level 2, and so on. Level 0 is always assigned to the FCs that retrieve the drones. Each path in the network corresponds to a route. It starts in a copy of the FCs in some level (from 2 to N) and ends in a copy of the FCs visited in Level 0. Since two distinct drones cannot visit the same customer, each customer cannot be visited in different levels.

Fig. 3 illustrates the multi-layer network for the example in Fig. 1.

By using the notation reported in Table 2, the mathematical model can be formulated as follows.

$$\min \sum_{i\in V}\sum_{\substack{c\in C\\ c\neq i}}\sum_{r\in L} r\, t_{ic}\, y^r_{ic} \tag{1}$$

$$\sum_{r\in L} x^r_i = 1 \qquad \forall i \in C \tag{2}$$

$$\sum_{s\in D}\sum_{j\in C}\sum_{\substack{r\in L\\ r\neq 1}} y^r_{sj} = k \tag{3}$$

$$\sum_{i\in C} x^1_i = k \tag{4}$$

$$\sum_{\substack{j\in C\\ j\neq i}} y^r_{ij} = x^{r+1}_i \qquad \forall i \in C, \forall r \in L, r \neq N \tag{5}$$

$$\sum_{s\in D} y^0_{js} = x^1_j \qquad \forall j \in C \tag{6}$$

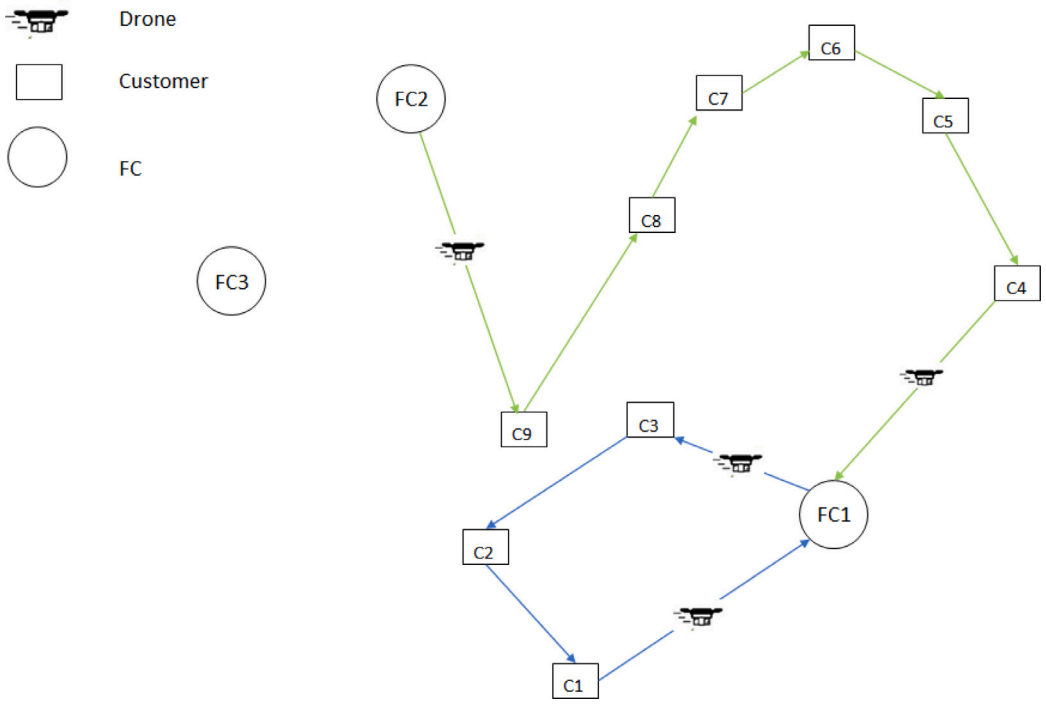

Fig. 1. Example.

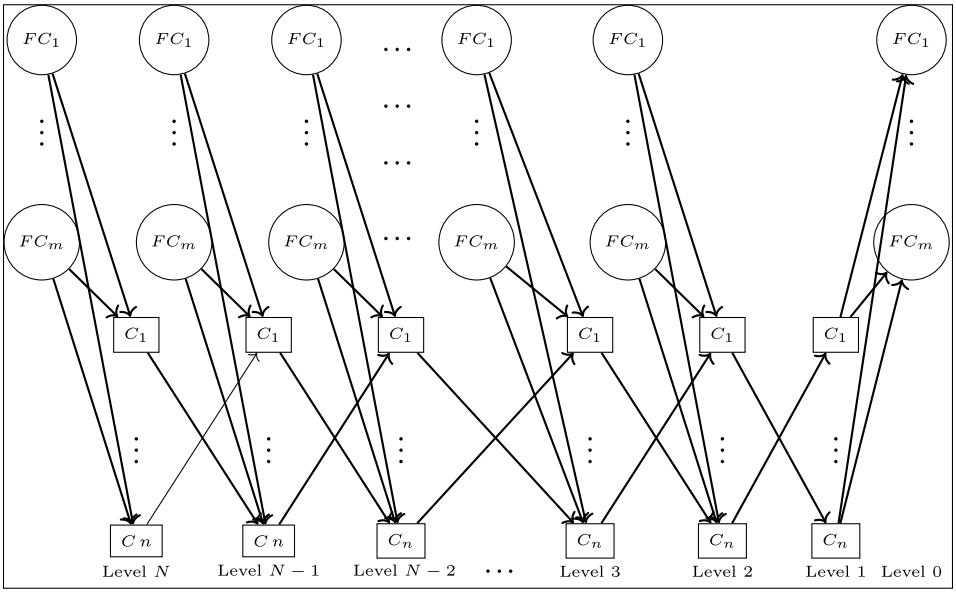

Fig. 2. Multi-layer network for the DLLRP.

$$\sum_{\substack{i\in V\\ i\neq j}} y_{ij}^{r} = x_j^{r} \qquad \forall j \in C, \forall r \in L, r \neq N \tag{7}$$

$$\sum_{s\in D} y_{sj}^{N} = x_j^{N} \qquad \forall j \in C \tag{8}$$

$$z_s \geq y_{sj}^{r} \qquad \forall s \in D, \forall j \in C, \forall r \in L, r \neq 1 \tag{9}$$

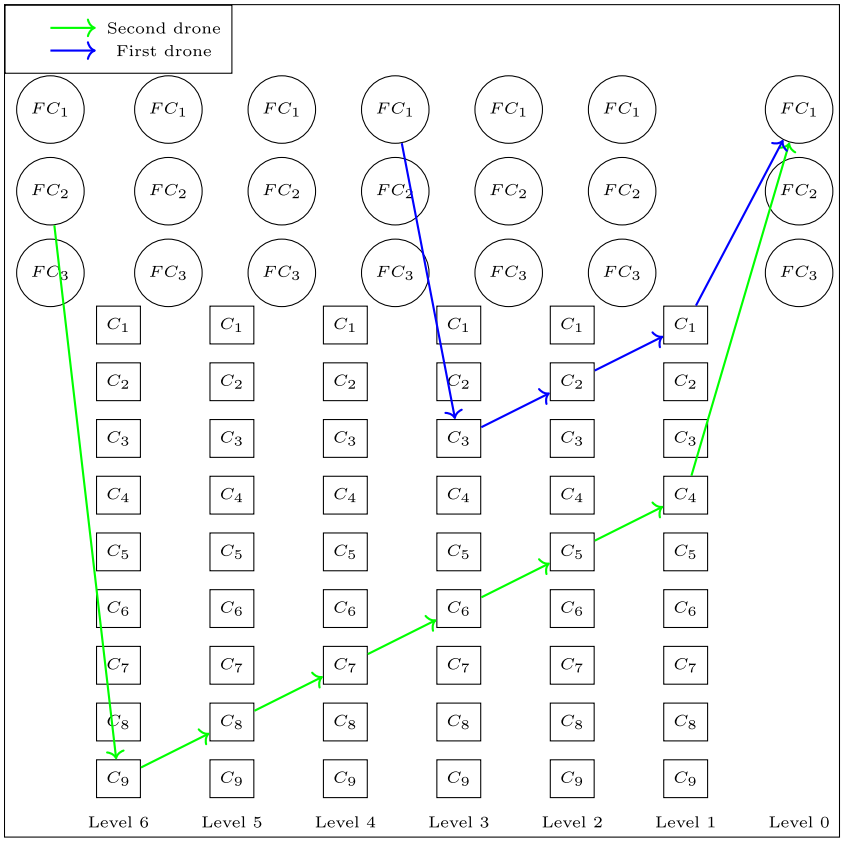

Fig. 3. Multi-layer network corresponding to the solution of Fig. 1.

Table 2
Notation for the mathematical model for the DLLRP.

Sets	
$C = \{C_1, \dots, C_n\}$	Set of customers indexed by c
$D = \{FC_1, \dots, FC_m\}$	Set of FCs, indexed by s
$V = C \cup D$	Set of all nodes indexed by i, j
$L = \{0, 1, \dots, N\}$	Set of levels, indexed by r
Parameters	
k	Number of drones
Q	Drone payload capacity
DS	Maximum number of FCs
d_j	Demand of customer $j \in C$
t_{ij}	Flight time along arc (i, j)
ϕ	Maximum number of drones that can be hosted in each FC
B	Drone battery capacity
M_{sj}, M'_{ij}	Big-M parameters
Decision variables	
x_i^r	Binary variable that takes 1 if customer i is visited in level r; otherwise, 0.
y_{ij}^r	Binary variable that takes 1 if node j is visited right after node i and there are exactly r nodes left to be visited after (including node j); otherwise, 0.
e_i	Accumulated energy consumption upon arrival at node $i \in V$
z_s	Binary variable that takes 1 if FC s is used; otherwise, 0.
u_{ij}	Total load carried by the drone while traveling over arc (i, j) after serving customer i.
v_{sj}	Total load carried by the drone traveling over arc (s, j) upon departure from FC s.

$$\sum_{s\in D} z_s \le DS \tag{10}$$

$$\sum_{j\in C}\sum_{r\in L} y^r_{sj} \le \phi \qquad \forall s \in D \tag{11}$$

$$y^0_{is} \le \sum_{\substack{r\in L\\ r\neq 1}}\sum_{j\in C} y^r_{sj} \qquad \forall i \in C, \forall s \in D \tag{12}$$

$$v_{sj} \ge d_j \sum_{\substack{r\in L\\ r\neq 1}} y^r_{sj} \qquad \forall s \in D, \forall j \in C \tag{13}$$

$$v_{sj} \le Q \sum_{\substack{r\in L\\ r\neq 1}} y^r_{sj} \qquad \forall s \in D, \forall j \in C \tag{14}$$

$$u_{ij} \ge d_j \sum_{\substack{r\in L\\ r\neq N}} y^r_{ij} \qquad \forall i, j \in C, i \neq j \tag{15}$$

$$u_{ij} \le (Q - d_i) \sum_{\substack{r\in L\\ r\neq N}} y^r_{ij} \qquad \forall i, j \in C, i \neq j \tag{16}$$

$$\sum_{s\in D} v_{si} + \sum_{\substack{j\in C\\ j\neq i}} u_{ji} - \sum_{\substack{j\in C\\ j\neq i}} u_{ij} = d_i \qquad \forall i \in C \tag{17}$$

$$e_s + k'(W + M + v_{sj})^{3/2} t_{sj} \le e_j + M_{sj}(1 - \sum_{\substack{r\in L\\ r\neq 1}} y^r_{sj}) \qquad \forall s \in D, \forall j \in C \tag{18}$$

$$e_i + k'(W + M + u_{ij})^{3/2} t_{ij} \le e_j + M'_{ij}(1 - \sum_{\substack{r\in L\\ r\neq N}} y^r_{ij}) \qquad \forall i, j \in C, i \neq j \tag{19}$$

$$e_j + k'(W + M)^{3/2} \sum_{s\in D} t_{js} y^0_{js} \le B \qquad \forall j \in C \tag{20}$$

$$e_s = 0 \qquad \forall s \in D \tag{21}$$

$$z_s \in \{0, 1\} \qquad \forall s \in D \tag{22}$$

$$x^r_i \in \{0, 1\} \qquad \forall i \in C, \forall r \in L \tag{23}$$

$$y^r_{cj} \in \{0, 1\} \qquad \forall c \in C, \forall j \in V, c \neq j, \forall r \in L, r \neq N \tag{24}$$

$$y^r_{sj} \in \{0, 1\} \qquad \forall s \in D, \forall j \in C, \forall r \in L, r \neq 1 \tag{25}$$

$$v_{sj} \ge 0 \qquad \forall s \in D, \forall j \in C \tag{26}$$

$$u_{ij} \ge 0 \qquad \forall i, j \in C, i \neq j \tag{27}$$

$$e_i \ge 0 \qquad \forall i \in C \tag{28}$$

The objective function (1) minimizes the total latency, defined as the sum of customers' waiting times. Constraints (2) ensure that each customer is visited exactly once. Constraint (3) ensures to dispatch exactly k drones. Constraint (4) guarantees that all the dispatched drones are finally retrieved. Constraints (5)–(8) represent the connectivity constraints. Constraints (9) mark a FC as used, when a drone is launched from it. Constraint (10) limits the number of FCs to use and constraints (11) avoid the FCs capacity to be violated. Constraints (12) ensure that only FCs already used to launch one or more drones. We recall that drone launch and collection can possibly take place at two distinct FCs. Constraints (12) ensure that only FCs already used to launch one or more drones can be used to retrieve drones. Constraints (13)–(17) model the restrictions on drone payload capacity. Constraints (13) and (15) determine the minimum values for v_{sj} and u_{ij} and allow to estimate the minimum capacity required to carry the demand of customer j. Constraints (14) and (16) force the same variables to be zero whenever variables y^r_{sj} and y^r_{ij} are zero, respectively. Also, they ensure that the drone maximum capacity Q is not violated. Note that $(Q - d_i)$ is an upper bound on the total demand of customers to be visited after customer i. Constraints (18) consider the energy consumption between a FC $s \in D$ and the customer $j \in C$ visited right after. In a similar way, constraints (19) account for the energy consumed while traveling between two consecutive customers $i, j \in C$. Constraints (20) ensure that the drone battery capacity is respected. Here, the energy consumed to reach the final FC $s \in D$ is added. Finally, constraints (22)–(28) establish the nature of the variables.

Constraints (18)–(21) are derived from the energy consumption model proposed by Dorling et al. (2016), which is based on the assumption that thrust balances the weight force and that the power consumed during takeoff or landing is approximately equivalent to the power consumed while hovering. Under these assumptions, the power consumption P (in watts W) of a H-rotor drone that flies over arc (i, j), upon departing from customer i while carrying a load of l_{ij}, can be evaluated as:

$$P(l_{ij}) = \sqrt{\frac{g^3}{2\tau\kappa H}}(W + M + l_{ij})^{3/2} \tag{29}$$

where W is the frame weight of drone (kg) and M is the drone battery weight (kg); g represents the gravity (N); τ is the fluid density of air (kg/m^3); κ is the area of the spinning blade disc (m^2), and H is the number of drone rotors. Also note that the drone load l_{ij} is specified as follows:

$$l_{ij} = \begin{cases} v_{ij} & i \in D,\ j \in C \\ u_{ij} & i \in C,\ j \in C \\ 0 & i \in C,\ j \in D \end{cases}$$

From now on, for the sake of brevity, we denote $\sqrt{\frac{g^3}{2\tau\kappa H}}$ by k'.

Therefore, the energy consumption E along arc (i,j) traversed in time t_{ij} (in Watt-second) is represented as:

$$E(l_{ij}, t_{ij}) = \sqrt{\frac{g^3}{2\tau\kappa H}}(W + M + l_{ij})^{3/2} t_{ij} \tag{30}$$

Clearly, the energy consumption nonlinearly depends on the load upon departure from each node.

3.1. Robust energy consumption constraint

In this section, we describe how uncertainty in flight times can be incorporated into the model via a robust optimization approach. This framework is particularly suitable for this problem as it explicitly balances solution quality and feasibility under worst-case scenarios. Although this conservatism may appear restrictive, it is appropriate in our case, given the limited battery autonomy of drones: unexpected energy consumption fluctuations could even lead to drone crashes. It is evident, then, the tremendous impact that ignoring uncertainty could have, especially in a context where routing decisions should be taken, as in the present paper.

Let us consider an arbitrary route π represented by the ordered set of arcs (i,j), including the starting FC, the set of visited customers, and the ending FC. We can denote the total drone energy consumption along the route by:

$$C(t, \pi) = \sum_{(i,j)\in\pi} k'(W + M + l_{ij})^{3/2} t_{ij}. \tag{31}$$

We should note that $C(t,\pi)$ is a convex function in l_{ij}, since $k'(W + M + l_{ij})^{3/2}$ is convex in l_{ij} and the flight time t_{ij} is positive. Let us assume that the vector of flight times $\tilde{t} = [t_{ij}] \in \mathbb{R}^{L_1}$ is uncertain and belongs to the uncertainty set U

$$U = \{\tilde{t} = \bar{t} + \mathcal{T}\xi | \xi \in \mathcal{Z} \subseteq \mathbb{R}^{L_2}\}. \tag{32}$$

Here $\bar{t} \in \mathbb{R}^{L_1}$ is the nominal value, $\mathcal{T} = [\hat{t}_1, \hat{t}_2, \ldots, \hat{t}_{L_2}] \in \mathbb{R}^{L_1 \times L_2}$ is a given column-wise matrix and ξ represents the vector of primitive uncertainties. Depending on how the set $\mathcal{Z}$ is defined, different uncertainty regions can be considered. For instance, ellipsoidal and box uncertainty sets correspond to $\mathcal{Z} = \{\xi | \|\xi\|_p \le \rho\}$ with $p = 2$ and $p = \infty$, respectively, where $\|\cdot\|_p$ is the p-norm (Ben-Tal et al., 2015) . We assume that the set $\mathcal{Z}$ is nonempty, convex, and compact, $0 \in ri(\mathcal{Z})$ where $ri(\mathcal{Z})$ denotes the relative interior of $\mathcal{Z}$. The energy feasibility constraint under uncertainty becomes a nonlinear constraint with robust parameters:

$$C(\tilde{t}, \pi) \le B, \quad \forall \tilde{t} \in U. \tag{33}$$

Proposition 1. *If we consider ellipsoidal and interval uncertainty sets, the nonlinear robust energy feasibility constraints (33) can be rewritten as*

$$\sum_{(i,j)\in\pi} k'(W + M + l_{ij})^{3/2} \bar{t}_{ij} + \rho \left\| \sum_{(i,j)\in\pi} k'(W + M + l_{ij})^{3/2} \hat{t}_{ij} \right\|_q \le B \tag{34}$$

where $\rho \in \mathbb{R}$ is an input parameter specified by the decision maker controlling robustness in $\mathcal{Z}$ and q is such that $\frac{1}{p} + \frac{1}{q} = 1$.

Proof. As shown by Ben-Tal et al. (2015) (Theorem 2) constraint (33) is satisfied if and only if

$$\bar{t}^T \lambda + \delta^*(\mathcal{T}^T \lambda | \mathcal{Z}) - C_*(\lambda, \pi) \le B \tag{35}$$

where $\lambda \in \mathbb{R}^{L_1}$, $\delta^*(\psi|S) = \sup_{\mu\in S} \psi^T \mu$ is the support function of the arbitrary set S, and C_* denotes the conjugate of function C which is defined as

$$C_*(\lambda, \pi) = \inf_{\tilde{t}\in\mathbb{R}^{L_1}} \{\tilde{t}^T \lambda - C(\tilde{t}, \pi)\}. \tag{36}$$

In our case, the support function δ^* simplifies to $\delta^*(\mathcal{T}^T\lambda|\mathcal{Z}) = \rho \|\mathcal{T}^T\lambda\|_q$.

Therefore, (35) reduces to

$$\bar{t}^T \lambda + \rho \|\mathcal{T}^T \lambda\|_q - C_*(\lambda, \pi) \le B \tag{37}$$

Clearly, $C(\tilde{t}, \pi)$ is linear in terms of the robust vector $\tilde{t}$ and it can easily be verified that

$$C_*(\lambda, \pi) = \begin{cases} 0, & \lambda = [\sum_{(i,j)\in\pi} k'(W + M + l_{ij})^{3/2}] \\ -\infty, & \lambda \ne [\sum_{(i,j)\in\pi} k'(W + M + l_{ij})^{3/2}] \end{cases}$$

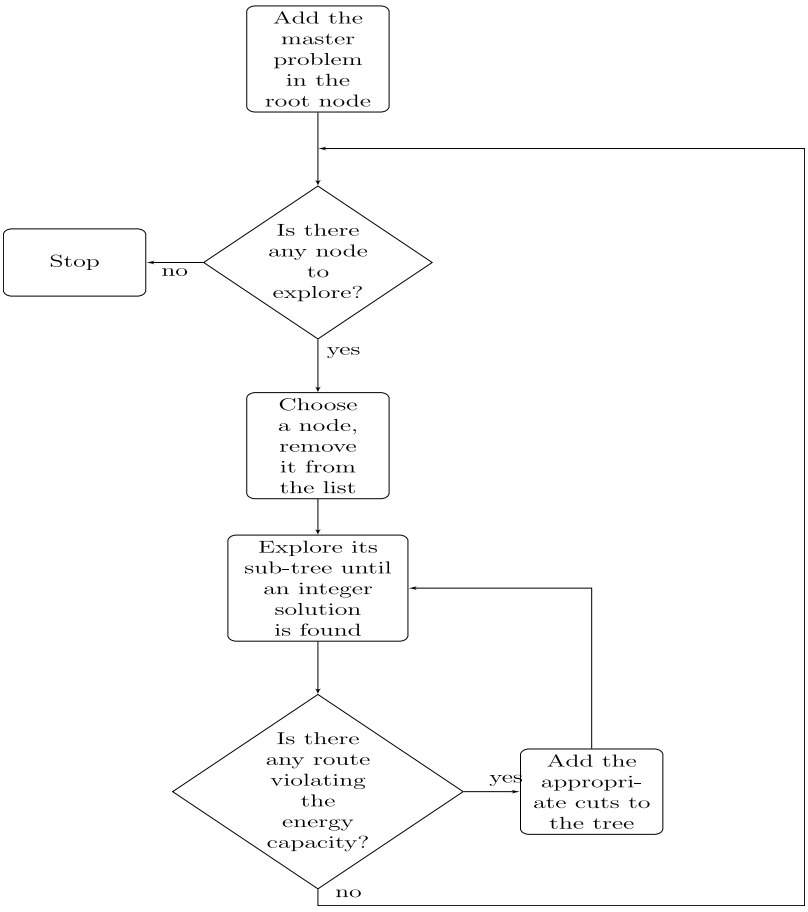

Fig. 4. Overview of the B&Ck algorithm.

Hence, the deterministic counterpart of (33) is derived as

$$\sum_{(i,j)\in\pi} k'(W+M+l_{ij})^{3/2}\bar{t}_{ij} + \rho\left\|\sum_{(i,j)\in\pi} k'(W+M+l_{ij})^{3/2}\hat{t}_{ij}\right\|_q \leq B \tag{38}$$

Moreover, flight time uncertainty also affects the objective function (1). For the box uncertainty set ($p = \infty$, $q = 1$), its deterministic counterpart can be rewritten as follows:

$$\min \sum_{i\in V}\sum_{\substack{c\in C\\ c\neq i}}\sum_{r\in L} r\,\bar{t}_{ic}\,y^r_{ic} + \rho\Big(\sum_{i\in V}\sum_{\substack{c\in C\\ c\neq i}}\sum_{r\in L} r\,\hat{t}_{ic}\,y^r_{ic}\Big) \tag{39}$$

For the ellipsoidal uncertainty set ($p = q = 2$), the deterministic counterpart is expressed as follows:

$$\min \sum_{i\in V}\sum_{\substack{c\in C\\ c\neq i}}\sum_{r\in L} r\,\bar{t}_{ic}\,y^r_{ic} + \rho\sqrt{\sum_{i\in V}\sum_{\substack{c\in C\\ c\neq i}}\sum_{r\in L} r^2\,Var(\tilde{t}_{ic})\,y^r_{ic} + 2\sum_{i\in V}\sum_{\substack{c\in C\\ c\neq i}}\sum_{r\in L}\sum_{\substack{i'\in V\\ i'\neq i}}\sum_{\substack{c'\in C\\ c'\neq c\\ c'\neq i'}}\sum_{r'\in L} r\,r'\,COV(\tilde{t}_{ic},\tilde{t}_{i'c'})y^r_{ic}y^{r'}_{i'c'}} \tag{40}$$

The NP-hardness of the DLLRP, as a location routing problem, and the presence of nonlinear constraints (also nonlinear objective function in case of ellipsoidal uncertainty set) call for the design of a tailored solution method able to tackle the problem at hand.

4. Solution approach

In this Section, we present an efficient exact method to address the computational difficulty of the DLLRP. In particular, we propose a Branch&Check (B&Ck, for short) algorithm. B&Ck (Beck, 2010; Thorsteinsson, 2001) is a form of logic-based Benders

decomposition approach (Bruni et al., 2022), which divides a problem into a Master Problem (MP) and a subproblem. The MP is very often obtained by ignoring or relaxing difficult constraints of the problem. The main difference between logic-based Benders and B&Ck is that in the logic-based Benders approach, the subproblems are optimization problems to be solved, whereas, in the B&Ck, the subproblem only checks specific aspects of the problem, very often the feasibility of the MP solution with respect to the original problem constraints. If the subproblem is infeasible, one or more cuts are added to the MP, with the aim of excluding the current solution, or solutions with an identifiable infeasible pattern. Conflict analysis from constraint programming can also be used to generate cuts and fix variables in the MP through propagation. The algorithm iterates between the MP and the subproblem until a globally optimal solution is found. In the B&Ck, the subproblems are solved during the search for a solution to the MP, without waiting until the MP is solved to optimality, and cuts are generated and added at each feasible MP solution. In this paper, we apply the B&Ck, on a MP whose constraints set is defined by (2)–(17) and (22)–(27). We notice that the nonlinear energy consumption constraints are not included in the MP. Under the box uncertainty set, the MP objective function is (39); for the ellipsoidal case, the MP objective function is (40). The objective function is then linear for the box uncertainty set and instead nonlinear when the ellipsoidal uncertainty set is considered. In both cases, the MP has linear constraints and mixed-integer variables. Hence, a Branch&Bound (B&B) method is used to explore the decision tree and, at each integer solution found in the B&B tree, the (global) feasibility of the solution is checked. Fig. 4 shows the flowchart of the proposed B&Ck algorithm.

Once an integer feasible solution is found, a procedure is invoked to check the feasibility of the master problem solution with respect to the energy constraints. More in detail, for each of the k drone routes π_p, $p = 1, \dots, k$ identified by the current master problem solution, the energy consumption constraints (34) are checked to know whether or not the energy consumed by the drone is enough to complete the route. Algorithm 1 describes the pseudocode of the procedure invoked, through a callback procedure, to build the k drone routes starting from the information encoded into the decision variables of the master problem. In particular, after having set the Boolean variable $flag$ to false, and the set of eligible nodes $C = C$, the algorithm starts with an empty route in line 3, looking for the last customers visited (at level 1) by one of the drones, i.e. $c \in C$ such that $x_c^1 = 1$. This customer is followed by the FC $s \in D$ such that $y_{cs}^0 = 1$ (line 9), where the drone is finally retrieved. The arc (c, d) is then inserted at the end of the list π_p (line 10). Then, iteratively, in lines 12–19 the customer visited before the current node c' is found, and the arc (c', c) is inserted at the beginning of the list π_p. Next, c' becomes the current node and the process is repeated until the first customer visited is found. If this is the case, the Boolean variable $flag$ is set to one and, in line 21, the launching FC is found ($s \in D$, $\sum_{r \in L} y_{sc}^r = 1$) and the arc (d, c) inserted at the beginning of the list π_p. The algorithm finally ends by returning all the routes in line 24.

Algorithm 1: Pseudocode for the build route procedure

```
1  flag ← 0, C ← C
2  for p = 1 ... k do
3      π_p ← ∅
4      for c ∈ C do
5          if x_c^1 = 1 then
6              break
7          end
8      end
9      d ← {s ∈ D | y_cs^0 = 1}
10     Insert {(c, d)} in π_p
11     C ← C \ {c}
12     repeat
13         c' ← {i ∈ C | Σ_{r∈L} y_ic^r = 1}
14         if c' = null then
15             flag ← 1
16             break;
17         end
18         Insert {(c', c)} at the beginning of π_p
19         c ← c'
20     until flag = 0;
21     d ← {s ∈ D | Σ_{r∈L} y_sc^r = 1}
22     Insert {(d, c)} at the beginning of π_p
23 end
24 return {π_p}_{p=1}^k
```

Let π be one of the routes retrieved by the build route procedure, the total energy consumption over π, under the box uncertainty set assumption, is expressed as

$$C(\tilde{t}, \pi) = \sum_{(i,j) \in \pi} k'(W + M + l_{ij})^{3/2}(\bar{t}_{ij} + \rho \hat{t}_{ij}). \tag{41}$$

Table 3
Example data.

Node	X	Y	Demand
C_1	163	181	0.3
C_2	629	128	0.4
C_3	619	218	0.7
C_4	92	842	0.6
FC_1	335	846	–
FC_2	631	307	–

For the ellipsoidal case, the total energy consumption over π is expressed as

$$C(\tilde{t},\pi) = \sum_{(i,j)\in\pi} k'(W+M+l_{ij})^{3/2}\bar{t}_{ij} + \rho\left[\sum_{(i,j)\in\pi} k'^2(W+M+l_{ij})^3\, Var(\tilde{t}_{ij}) + 2\sum_{(i,j)\in\pi}\sum_{\substack{(i',j')\in\pi\\(i',j')\neq(i,j)}} k'^2(W+M+l_{ij})^{3/2}(W+M+l_{i'j'})^{3/2}\, COV(\tilde{t}_{ij},\tilde{t}_{i'j'})\right]^{1/2} \quad (42)$$

If $\{\pi_p\}_{p=1}^{k}$ are feasible, the incumbent can eventually be updated. If a route violates the energy constraint, a valid feasibility cut is generated and added to the MP as lazy constraints. In particular, based on the general idea of "no-good" cuts as described in Balas and Jeroslow (1972), we add a "no-good" cut for each energy infeasible route. Notice that, this is stronger than excluding the current integer solution just by adding a single no-good cut.

The valid cut $\mathcal{NG}(\pi)$ corresponding to route π is defined as follows

$$\mathcal{NG}(\pi) = \sum_{(i,j)\in\pi}\sum_{r\in L}(1-y^r_{ij}) \geq 1. \quad (43)$$

This globally valid cut ensures that, for each violated route, at least one customer/FC is removed. Since the feasible region of the original problem is bounded and there is a finite number of feasible solutions, the number of such "no-good" cuts is also limited guaranteeing the algorithm convergence. If all the nodes are explored and none of them passes the feasibility check in terms of energy consumption, we can conclude that the problem is infeasible.

In the following, we present a small example to clarify how the B&Ck algorithm works.

4.1. Illustrative example

Consider a small example with four customers, two drones, and two potential FCs, each with a capacity of two. Table 3 shows the coordinates of the customers $C1$, $C2$, $C3$, $C4$ and the potential FCs in the two-dimensional space, and the customers' demands (in terms of parcel weight). Let us consider an ellipsoidal uncertainty set with correlated flight times (Appendix reports the covariance matrix). A drone with a battery of 0.30 kWh is considered.[1] Fig. 5 displays different solutions obtained in each iteration of the B&Ck algorithm. The objective value of the solution and the amount of energy consumed in each route are indicated by Obj and E, respectively.

In the first solution (Fig. 5(a)) the red route is not feasible with respect to the battery capacity (called energy infeasible) and the cut $y^2_{FC_2C_1} + y^1_{C_1C_4} + y^0_{C_4FC_2} \leq 2$ is added. The solutions in Iteration 1 and Iteration 2 are energy feasible and the incumbent is updated (see Figs. 5(b) and 5(c)). Again, at Iteration 3, an energy infeasible solution is obtained (Fig. 5(d)) that is cut off in the next iteration by adding cut $y^2_{FC_2C_3} + y^1_{C_3C_4} + y^0_{C_4FC_2} \leq 2$. At Iteration 4, a different solution is found which is, again, energy infeasible; therefore, the corresponding no-good cut $y^2_{FC_2C_2} + y^1_{C_2C_4} + y^0_{C_4FC_2} \leq 2$ is added to the master problem. By adding this cut at Iteration 5, an energy-feasible solution is obtained and the incumbent is also updated; since at this step, all the tree nodes are traversed, the current solution is the optimal one and the search ends.

5. Computational experiments

In this Section, we report the computational results carried out to assess the efficiency of the exact method. We validated our algorithm on a set of instances introduced by Cheng et al. (2020a). The A1 and A2 instances, were originally proposed for the single-depot deterministic drone routing problem (for A2 instances, the customers' coordinates were divided by 2 to make the problem feasible). We considered up to five FCs and two spatial configurations for the FCs: for type *Centered* instances, the FCs are located in the center of the delivery area, while for type *Marginal* instances, the FCs are located in the outskirts of the area. Table 4 shows the coordinates of the FCs under each configuration, where

$$\bar{X} = \frac{1}{n}\sum_{i\in C} X_i, \quad X_{min} = \min_{i\in C} X_i, \quad X_{max} = \max_{i\in C} X_i, \quad R_X = X_{max} - X_{min}$$

[1] The other parameters are equal to those reported in Section 5.

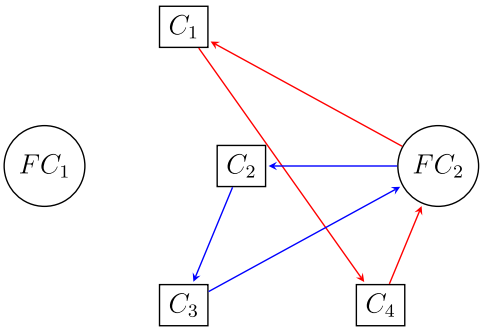

(a) Iteration 0: $Obj = 0.609, E = \{0.042, 0.390\}$ (Infeasible)

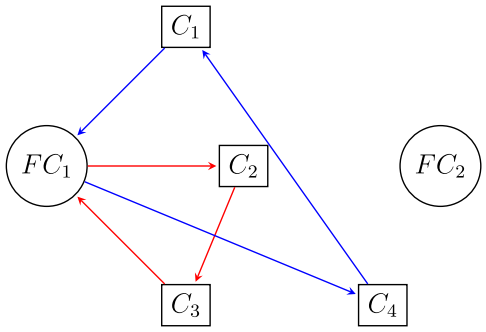

(b) Iteration 1: $Obj = 1.092, E = \{0.293, 0.244\}$ (feasible)

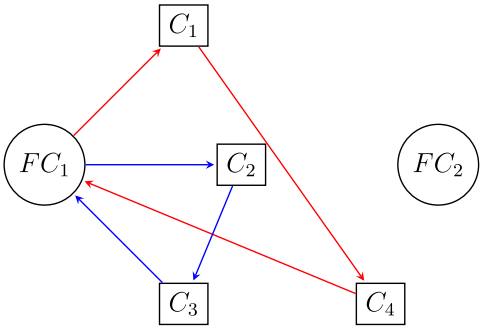

(c) Iteration 2: $Obj = 0.790, E = \{0.244, 0.293\}$ (feasible)

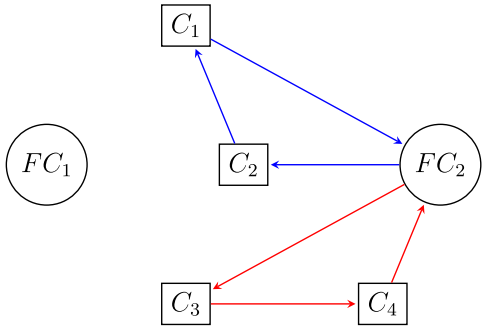

(d) Iteration 3: $Obj = 0.508, E = \{0.182, 0.345\}$ (infeasible)

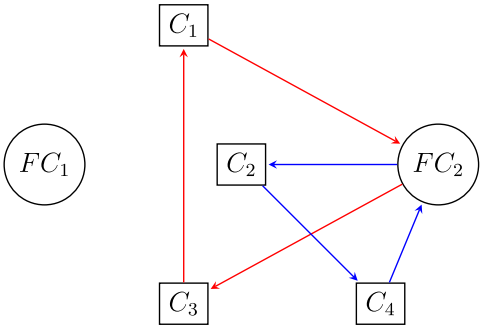

(e) Iteration 4: $Obj = 0.565, E = \{0.204, 0.348\}$ (infeasible)

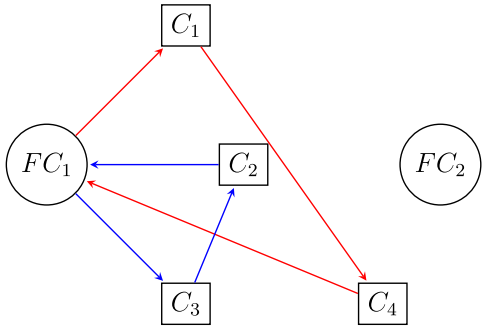

(f) Iteration 5: $Obj = 0.769, E = \{0.243, 0.293\}$ (optimal solution)

Fig. 5. Illustrative example: Iterations of the B&Ck algorithm.

Table 4
FC coordinates.

FC	*Centered*		*Marginal*	
	X	Y	X	Y
FC_1	$\bar{X}$	$\bar{Y}$	X_{min}	Y_{min}
FC_2	$\bar{X}$	$\bar{Y} - \delta R_Y$	X_{max}	Y_{min}
FC_3	$\bar{X}$	$\bar{Y} + \delta R_Y$	X_{min}	Y_{max}
FC_4	$\bar{X} - \delta R_X$	$\bar{Y}$	X_{max}	Y_{max}
FC_5	$\bar{X} + \delta R_X$	$\bar{Y}$	$\frac{X_{min}+X_{max}}{2}$	Y_{min}

$$\bar{Y} = \frac{1}{n}\sum_{i \in C} Y_i, \quad Y_{min} = \min_{i \in C} Y_i, \quad Y_{max} = \max_{i \in C} Y_i, \quad R_Y = Y_{max} - Y_{min} \tag{44}$$

and X_i, Y_i represent the coordinates of customer $i \in C$. The input parameter $\delta \in (0, 1)$, is a dispersion factor, set to 0.2 in all the experiments.

We considered Alta 8 drones with the following characteristics: $B = 0.355$ kWh, $W = 6.2$ kg, $M = 2.8$ kg, $Q = 9.1$ kg, $H = 8$, P = 1.204 kg/m^3. In (29), $\kappa = 0.1256$ m^2 and $g = 9.81$, N/kg.

Table 5
Results for A1 instances: box uncertainty set.

Instance	n	m	k	ϕ	*Centered*							*Marginal*						
					AOA[a]		B&Ck					AOA[a]		B&Ck				
					Obj	*CPU*	*Obj*	*CPU*	*#Cb*	*ΔOF%*	*ΔT%*	*Obj*	*CPU*	*Obj*	*CPU*	*#Cb*	*ΔOF%*	*ΔT%*	*Gap%*
Set_A_1_cust_10_1	10	5	2	2	2.016	7.09	2.016	1.14	39	0	83.92	1.635	2.85	1.635	1.02	40	0	64.21	
Set_A_1_cust_10_2					1.796	2.02	1.796	0.79	7	0	60.89	1.557	2.68	1.557	0.70	12	0	73.88	
Set_A_1_cust_10_3					1.838	4.11	1.838	3.21	84	0	21.90	1.400	3.02	1.400	1.50	5	0	50.33	
Set_A_1_cust_10_4					1.568	2.77	1.568	1.50	16	0	45.85	1.130	2.26	1.130	1.00	14	0	55.75	
Set_A_1_cust_10_5					1.956	2.75	1.956	1.32	11	0	52.00	1.860	3.31	1.860	1.24	21	0	62.54	
Set_A_1_cust_15_1	15	5	3	2	2.090	33.38	2.090	5.42	7	0	83.76	2.050	35.10	2.050	4.30	1	0	87.75	
Set_A_1_cust_15_2					2.524	48.49	2.524	5.53	6	0	88.60	2.252	30.17	2.252	5.33	3	0	82.33	
Set_A_1_cust_15_3					1.999	37.94	1.999	5.50	9	0	85.50	2.127	32.12	2.127	5.74	7	0	82.13	
Set_A_1_cust_15_4					2.241	42.86	2.241	4.68	8	0	89.08	2.346	41.78	2.346	4.50	8	0	89.23	
Set_A_1_cust_15_5					2.350	47.55	2.350	5.40	9	0	88.64	1.873	51.74	1.873	4.04	5	0	92.19	
Set_A_1_cust_20_1	20	5	4	3	2.602	336.83	2.602	12.83	12	0	96.19	2.591	305.37	2.591	15.46	8	0	94.94	
Set_A_1_cust_20_2					2.667	442.88	2.667	10.62	7	0	97.60	2.559	440.93	2.559	13.53	15	0	96.93	
Set_A_1_cust_20_3					2.680	496.25	2.680	10.32	5	0	97.92	2.684	425.31	2.684	11.35	7	0	97.33	
Set_A_1_cust_20_4					–	500	2.383	9.16	4	–	98.17	–	500	2.492	13.43	13	–	97.31	
Set_A_1_cust_20_5					–	500	2.707	11.81	10	–	97.64	–	500	2.828	10.87	6	–	97.83	
Set_A_1_cust_25_1	25	5	7	5	–	500	2.558	3.05	7	–	99.39	–	500	2.729	4.84	2	–	99.03	
Set_A_1_cust_25_2					–	500	3.055	3.45	14	–	99.31	–	500	3.156	6.36	4	–	98.73	
Set_A_1_cust_25_3					–	500	2.637	3.16	5	–	99.37	–	500	2.858	4.88	5	–	99.02	
Set_A_1_cust_25_4					–	500	2.831	4.17	10	–	99.17	–	500	2.776	3.23	6	–	99.35	
Set_A_1_cust_25_5					–	500	2.941	5.54	4	–	98.89	–	500	2.859	3.35	4	–	99.33	
Set_A_1_cust_30_1	30	5	8	6	–	500	3.602	4.85	4	–	99.03	–	500	3.546	8.04	9	–	98.39	
Set_A_1_cust_30_2					–	500	2.973	7.32	4	–	98.54	–	500	3.485	5.39	3	–	98.92	
Set_A_1_cust_30_3					–	500	3.070	5.77	4	–	98.85	–	500	3.921	6.49	6	–	98.70	
Set_A_1_cust_30_4					–	500	3.188	5.76	7	–	98.85	–	500	3.654	5.70	7	–	98.86	
Set_A_1_cust_30_5					–	500	3.087	5.76	2	–	98.85	–	500	4.029	6.55	7	–	98.69	
Avg.						300.20		5.52	12		87.12		354.72		47.71			88.55	

[a] These AOA results already appeared in Bruni and Khodaparasti (2022).

Let us denote with $\bar{d} = \frac{1}{k}\sum_{i=1}^{n} d_i$ the average load carried by each drone upon departing from the FC; with $Y = \lceil \frac{n}{k} \rceil$ an estimate of the average number of customers served by each drone, with $\zeta = \frac{\bar{d}}{Y}$ the average demand. Let also $\bar{t}_{ij}$ be the nominal value for the flight time (set equal to the flight distance as in Cheng et al. (2020a)) and $\hat{t}_{ij}$ be the peak value. Then,

$$\bar{C} = \beta\Big[k'(W+M+\bar{d})^{\frac{3}{2}}\frac{\sum_{i=1}^{m}\sum_{j=1}^{n}\bar{t}_{ij}}{m\,n} + \sum_{p=2}^{Y} k'(W+M+\bar{d}-(p-1)\zeta)^{\frac{3}{2}}\frac{\sum_{i=1}^{n}\sum_{j=1}^{n}\bar{t}_{ij}}{n(n-1)} + k'(W+M)^{\frac{3}{2}}\frac{\sum_{i=1}^{n}\sum_{j=1}^{m}\bar{t}_{ij}}{m\,n}\Big] \tag{45}$$

is the average energy consumption and

$$\hat{C} = \beta\Big[k'(W+M+\bar{d})^{\frac{3}{2}}\frac{\sum_{i=1}^{m}\sum_{j=1}^{n}\hat{t}_{ij}}{m\,n} + \sum_{p=2}^{Y} k'(W+M+\bar{d}-(p-1)\zeta)^{\frac{3}{2}}\frac{\sum_{i=1}^{n}\sum_{j=1}^{n}\hat{t}_{ij}}{n(n-1)} + k'(W+M)^{\frac{3}{2}}\frac{\sum_{i=1}^{n}\sum_{j=1}^{m}\hat{t}_{ij}}{m\,n}\Big] \tag{46}$$

the peak value.

We set the radius of the uncertainty set to $\rho = \lceil \bar{\rho} \rceil$, where $\bar{\rho}$ is the largest ρ that satisfies

$$\frac{\bar{C} + \rho\hat{C}}{B} \leq \Phi. \tag{47}$$

The parameter $\beta \in (0,1)$ and $\Phi \in [0,1]$ were empirically set to $\beta = 0.45$ and $\Phi = 0.92$, to make the problem challenging.

The number of levels N was determined by ordering the demands of customers in ascending order. Then, starting from the first element, the customers' demands were added one by one until the drone capacity was reached. Then, N was set equal to the number of orders added, which is clearly an upper bound for the number of customers visited in a route.

5.1. Performance of the B&Ck approach

All the experiments were executed on an Intel Core i7-10750H, with 2.60 GHz CPU and 16 GB RAM working under Windows 10. We compared the performance of the B&Ck algorithm (implemented using the algebraic modeling language AIMMS 4.79.2.5. and

Table 6
Results for A2 instances: box uncertainty set.

Instance	n	m	k	ϕ	*Centered*							*Marginal*							
					AOA		B&Ck					AOA		B&Ck					
					Obj	CPU	Obj	CPU	$\#Cb$	$\Delta OF\%$	$\Delta T\%$	Obj	CPU	Obj	CPU	$\#Cb$	$\Delta OF\%$	$\Delta T\%$	$Gap\%$
Set_A2_cust_10_1	10	5	2	2	1.901	2.51	1.901	0.45	9	0	82.07	1.759	2.16	1.759	1.37	20	0	36.57	
Set_A2_cust_10_2					1.712	2.68	1.712	0.63	8	0	76.49	–	500	2.270	500	3179	–	–	2.19
Set_A2_cust_10_3					1.787	2.05	1.787	1.21	20	0	40.98	–	500	2.313	500	3545	–	–	1.77
Set_A2_cust_10_4					1.808	2.13	1.808	1.17	17	0	45.07	–	500	3.413	500	3600	–	–	60.12
Set_A2_cust_10_5					1.795	2.57	1.795	1.29	24	0	49.81	–	500	6.583	500	3109	–	–	66.33
Set_A2_cust_15_1	15	5	3	2	2.11	37.94	2.110	3.87	7	0	89.80	2.165	30.95	2.165	2.29	8	0	92.60	
Set_A2_cust_15_2					2.035	34.72	2.035	2.31	7	0	93.35	2.032	30.43	2.032	1.97	6	0	93.53	
Set_A2_cust_15_3					1.934	22.27	1.934	2.37	8	0	89.36	1.795	26.58	1.795	2.89	9	0	89.13	
Set_A2_cust_15_4					2.313	47.91	2.313	2.17	8	0	95.47	2.247	41.05	2.247	1.93	5	0	95.30	
Set_A2_cust_15_5					2.108	20.58	2.108	2.55	7	0	87.61	2.342	20.6	2.342	2.19	14	0	89.37	
Set_A2_cust_20_1	20	5	4	3	2.312	302.21	2.312	4.70	9	0	98.44	2.791	273.28	2.791	4.92	10	0	98.20	
Set_A2_cust_20_2					2.625	452.68	2.625	7.53	59	0	98.34	2.163	434.08	2.163	5.42	8	0	98.75	
Set_A2_cust_20_3					2.425	451.64	2.425	4.05	6	0	99.10	2.561	403.01	2.561	4.24	2	0	98.95	
Set_A2_cust_20_4					–	500	2.866	4.12	3	–	99.18	–	500	3.098	4.88	12	–	99.02	
Set_A2_cust_20_5					–	500	2.101	4.61	8	–	99.08	–	500	3.470	5.54	93	–	98.89	
Set_A2_cust_25_1	25	5	7	5	–	500	2.957	1.13	3	–	99.77	–	500	2.920	2.00	11	–	99.60	
Set_A2_cust_25_2					–	500	2.957	1.20	7	–	99.76	–	500	2.920	1.23	2	–	99.75	
Set_A2_cust_25_3					–	500	2.605	1.34	2	–	99.73	–	500	2.822	1.51	1	–	99.70	
Set_A2_cust_25_4					–	500	2.811	1.14	4	–	99.77	–	500	2.944	1.29	2	–	99.74	
Set_A2_cust_25_5					–	500	2.584	1.19	10	–	99.76	–	500	3.658	1.31	2	–	99.74	
Set_A2_cust_30_1	30	5	8	6	–	500	3.095	2.12	6	–	99.58	–	500	3.532	2.12	4	–	99.58	
Set_A2_cust_30_2					–	500	3.370	1.88	5	–	99.62	–	500	3.502	3.09	19	–	99.38	
Set_A2_cust_30_3					–	500	3.452	2.29	8	–	99.54	–	500	3.140	4.15	12	–	99.17	
Set_A2_cust_30_4					–	500	3.590	4.25	17	–	99.15	–	500	3.928	2.17	5	–	99.57	
Set_A2_cust_30_5					–	500	3.408	2.81	12	–	99.44	–	500	3.477	2.10	13	–	99.58	
Avg.						295.28		2.50			89.61		365.09		64.94			94.58	32.60

using Gurobi 9.1. as the solver), with the AIMMS Outer Approximation (AOA) algorithm. The time limit for both algorithms was set to 500 s. The basic idea of the AOA method is to solve a sequence of nonlinear programming sub-problems and a relaxed mixed-integer linear master problem, where the nonlinear constraints are approximated by linear approximation. This solver has been proved to be the fastest (Kronqvist et al., 2019), also because it can benefit from different techniques integrated within mixed-integer linear solvers, such as Gurobi.

Tables 5 and 6 report the results under different FCs configurations for the box uncertainty case.

Columns 1–5 in Tables 5 and 6 show the characteristics of instances in terms of the number of customers, potential FCs, fleet size, and capacity of FCs. The best objective function found (if any, we report "-") is shown in columns with header Obj and the solution time in seconds in columns with header CPU and the number of callbacks in columns with header $\#Cb$. The performance of the B&Ck versus AOA is reported in terms of relative percentage gap ($\Delta OF = \frac{Obj_{B\&Ck} - Obj_{AOA}}{Obj_{AOA}} 100$) and percentage speed up rate $\Delta(T = \frac{|CPU_{B\&Ck} - CPU_{AOA}|}{CPU_{AOA}} 100)$. When the B&Ck is not able to optimally solve the instance within the time limit, the relative percentage gap $Gap\%$ with respect to the best LP bound of the MP is reported.

Starting from the *Centered* case for A1 instances, we observe that in half of the instances, the AOA fails to find any feasible solution within the time limit. Moreover, its solution time increases drastically with the increase in the problem size; the average CPU time for the instances solved to optimality with 10, 15, and 20 customers are respectively, 3.75, 42.04, and 425.32 s.

On the other hand, the B&Ck finds the optimal solution for all the instances, and, on average, is 13 times faster than AOA. For the *Marginal* setting, the AOA fails to find a feasible solution in 42% of cases. The average CPU time is 2.82 s for the 10-customers A1 instances, but rises to 390.54 s for the 20-customers instances. On the contrary, the B&Ck finds the optimal solution for all the A1 instances. In terms of solution time, the B&Ck outperforms the AOA with an average ΔT of 88.55%. In conclusion, AOA completely fails to provide any feasible solution for A1 instances with more than 25 customers. Regardless of the instance type and FC setting, the B&Ck algorithm outperforms AOA. Similar conclusions are drawn for the A2 instances: again, AOA fails to find any feasible solution for instances with more than 20 customers. In addition, the solution time for the 20-customers instances solved to optimality is quite high.

When we consider the more involved case of the ellipsoidal uncertainty set, also the objective function becomes nonlinear and the AOA fails in all the instances, hence the results are not reported in Tables 7 and 8.

The B&Ck finds the optimal solution for all A1 instances but one for the *Centered* configuration and the average CPU time is less than 134 s. For the *Marginal* configuration, in 20% of the cases, the B&Ck fails to find the optimal solution within the time limit but in 80% of such cases, the $Gap\%$ is limited to 3.29%. For the A2 instances with *Centered* FC configuration, the average CPU time is below 225 s; the B&Ck fails to solve to optimality six instances. For three of them, the $Gap\%$ is below 1%. For the *Marginal* configuration, the CPU time decreases to 164 s and the $Gap\%$, for the two instances not solved to optimality, is below 2.24%.

Table 7
Results for A1 instances: Ellipsoidal uncertainty set.

Instance	n	m	k	ϕ	*Centered*				*Marginal*			
					B&Ck				*B&Ck*			
					Obj	*CPU*	*#Cb*	*Gap%*	*Obj*	*CPU*	*#Cb*	*Gap%*
Set_A_1_cust_10_1	10	5	2	2	1.029	48.77	10		0.984	22.20	10	
Set_A_1_cust_10_2					1.116	36.68	9		1.090	12.87	14	
Set_A_1_cust_10_3					1.044	52.66	10		1.111	15.26	3	
Set_A_1_cust_10_4					0.926	20.59	3		1.042	8.17	8	
Set_A_1_cust_10_5					1.333	32.19	8		1.431	12.25	5	
Set_A_1_cust_15_1	15	5	3	2	1.201	87.68	4		1.172	58.40	5	
Set_A_1_cust_15_2					1.514	364.37	9		1.488	167.09	7	
Set_A_1_cust_15_3					1.161	154.85	3		1.425	161.71	6	
Set_A_1_cust_15_4					1.179	304.87	5		1.352	57.41	6	
Set_A_1_cust_15_5					1.354	376.50	6		1.220	61.17	5	
Set_A_1_cust_20_1	20	5	4	3	1.442	147.34	2		1.635	330.86	3	
Set_A_1_cust_20_2					1.507	500	3	15.71	1.653	500	3	1.67
Set_A_1_cust_20_3					1.483	141.32	7		1.773	500	1	43.98
Set_A_1_cust_20_4					1.511	75.89	6		1.619	500	8	1.36
Set_A_1_cust_20_5					1.512	197.13	10		1.874	500	6	3.29
Set_A_1_cust_25_1	25	5	7	5	1.410	54.62	18		1.716	118.78	34	
Set_A_1_cust_25_2					1.636	74.24	10		1.974	30.71	20	
Set_A_1_cust_25_3					1.428	41.66	16		1.833	500	23	0.81
Set_A_1_cust_25_4					1.578	60.35	16		1.724	62.13	21	
Set_A_1_cust_25_5					1.596	79.10	16		1.778	101.56	29	
Set_A_1_cust_30_1	30	5	8	6	1.921	49.32	14		2.172	59.02	15	
Set_A_1_cust_30_2					1.586	62.40	18		2.140	159.71	27	
Set_A_1_cust_30_3					1.646	78.77	16		2.411	386.58	22	
Set_A_1_cust_30_4					1.681	68.02	18		2.259	73.68	11	
Set_A_1_cust_30_5					1.646	239.13	17		2.490	114.69	17	
Avg.						133.94		15.71		180.57		10.22

Table 8
Results for A2 instances: Ellipsoidal uncertainty set.

Instance	n	m	k	ϕ	*Centered*				*Marginal*			
					B&Ck				*B&Ck*			
					Obj	*CPU*	*#Cb*	*Gap%*	*Obj*	*CPU*	*#Cb*	*Gap%*
Set_A2_cust_10_1	10	5	2	2	1.168	17.29	10		1.205	2.63	3	
Set_A2_cust_10_2					1.153	2.51	7		1.213	9.58	8	
Set_A2_cust_10_3					1.299	13.16	4		1.213	1.76	4	
Set_A2_cust_10_4					1.175	2.76	7		1.203	8.16	6	
Set_A2_cust_10_5					1.232	16.04	5		1.376	17.92	5	
Set_A2_cust_15_1	15	5	3	2	1.239	153.83	4		1.424	117.6	20	
Set_A2_cust_15_2					1.313	64.21	2		1.320	59.40	3	
Set_A2_cust_15_3					1.106	47.63	6		1.192	28.77	5	
Set_A2_cust_15_4					1.733	500	1	34.55	1.477	54.36	1	
Set_A2_cust_15_5					1.382	62.78	4		1.558	171.64	8	
Set_A2_cust_20_1	20	5	4	3	1.467	202.46	6		1.794	341.28	9	
Set_A2_cust_20_2					1.438	500	3	45.58	1.362	132.37	6	
Set_A2_cust_20_3					1.530	149.19	4		1.622	170.23	4	
Set_A2_cust_20_4					1.583	302.81	8		1.995	500	3	1.67
Set_A2_cust_20_5					1.182	335.58	5		2.011	500	13	2.24
Set_A2_cust_25_1	25	5	7	5	1.661	74.41	8		1.845	197.68	15	
Set_A2_cust_25_2					1.661	160.56	11		1.845	222.78	30	
Set_A2_cust_25_3					1.438	91.47	9		1.767	113.82	25	
Set_A2_cust_25_4					1.526	389.49	25		1.840	172.13	10	
Set_A2_cust_25_5					1.746	500	11	42.51	2.034	289.41	27	
Set_A2_cust_30_1	30	5	8	6	1.918	500	14	0.76	2.174	448.43	28	
Set_A2_cust_30_2					1.785	237.41	9		2.142	172.32	31	
Set_A2_cust_30_3					1.837	500	18	0.92	1.941	89.48	11	
Set_A2_cust_30_4					1.910	500	14	0.33	2.405	94.39	11	
Set_A2_cust_30_5					1.851	295.5	21		2.155	161.78	20	
Avg.						224.88		20.78		163.14		1.96

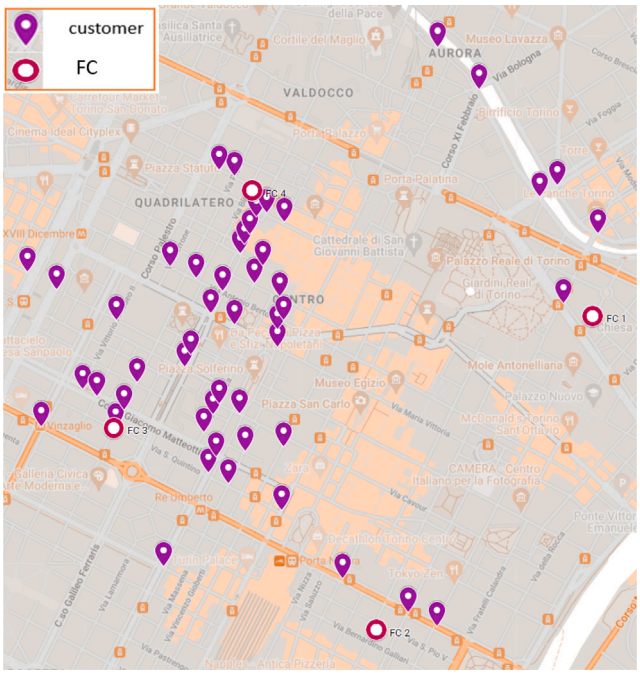

Fig. 6. Case study: location of customers and FCs.

6. Case study and managerial insights

In this Section, we present a case study on last-mile parcel delivery in Turin, Italy. Real sensitive data are anonymized and normalized by means of the data-fusion tool provided in Perboli et al. (2018a). The area considered (2.805×2.447 km^2) includes both the center of the city and a semi-central zone. The case study concerns the delivery of 50 orders with known delivery locations. Each order is a single parcel package that weighs between 0.2 and 1 kg (the average parcel weight is 0.6 kg). The orders are transferred from a distribution center in the outskirt of the city to four existing FCs, where the packages are loaded into a fleet of vehicles to perform the deliveries. Each FC can host up to two vehicles. Fig. 6 displays the spatial configuration of the customers and the FCs plotted in Google Maps.[2]

We considered three different fleet configurations: a homogeneous fleet of six drones, a homogeneous fleet of five Fuel-based Cargo Bikes (F-CB)s, and a homogeneous fleet of five Electric Cargo Bikes (E-CB)s. The drone maximum payload is five kilograms with a battery of 0.30 kWh. Cargo bikes have a payload capacity of seven kilograms. Real travel times are calculated by the Google Earth API and a georeference module (Wei, 2022), considering an average speed for a cargo bike of 20 km/h. In the case of drone delivery, the flight time is calculated as the Euclidean distance divided by the average drone speed of 40 km/h. The travel times can fluctuate up to 50%. We considered a service time of one minute for the drones. For the cargo bikes, the service time is longer (three minutes) because, upon arrival at the customer's location, the driver should park and secure the vehicle.

To investigate the effect of travel time uncertainty on the energy feasibility of the drone routes and the validity of the proposed model against a deterministic model, we have carried out a Monte Carlo simulation experiment. In particular, to assess the reliability of the solutions of both the robust and the deterministic model, we have generated 1000 different travel time scenario realizations lying in the uncertainty set U. For each scenario, and once fixed the values of the variables to the optimal solutions provided by the deterministic and the robust model, and the travel time values to the realizations associated to the given scenario, the energy consumption has been calculated according to the formula (31). For each scenario, this value has been then compared with the battery capacity to detect possible violations of the energy constrains. We have observed that the solution of the deterministic case is highly unreliable, since the energy consumed exceeds the battery capacity in the majority (76%) of the scenarios. On average, the deviation is around 3% but in the worst case it is around 14%. Unexpected battery depletion can cause the drone to prematurely return to the nearest FC for the battery replenishment, significantly disrupting the logistic process. It may also result in poor or lost connection and it can even lead to a drone crash. In this case, beside the safety issue, which is clearly the critical aspect, it should be considered the cost of the drone and its integrated equipment along with the incident recovery costs.

In order to provide managerial insights on environmental and economic aspects of drone-aided delivery, in comparison with more conventional delivery options, we have focused our analysis on customers' waiting time, annual costs, and CO_2-eq emissions.

[2] https://maps.google.com/.

Fig. 7. Optimal drone routes.

The waiting time and the total cost are, respectively, customer-oriented and server-oriented KPIs measuring the efficiency of the delivery system from the service user's and service provider's viewpoint. The level of CO_2-eq emissions assesses the environmental impact of the delivery. To obtain the results for the F-CB and the E-CB fleet, we solved the DLLRP without energy constraints. Figs. 7–8 display the optimal vehicle routes for different fleet configurations visualized by Google Earth Pro.[3]

Fig. 9 displays the customers' waiting time for each fleet configuration. As we can see, the use of drones allows a drastic reduction (by 70%) of the waiting time for the customers, compared to the CB configuration. This is due to the fact that terrestrial vehicles, such as CBs, travel on the road network which is affected by traffic congestion and it is also related to the shorter drone service time. The CBs route duration (related to drivers' work balance and vehicle depreciation cost Geromel Dotto and Thor Magnusson (2022), Huang et al. (2017) and Matl et al. (2018)) is around 50 min, but in the case of drones it drops to 13 min (see Fig. 10).

Fig. 11 displays the CO_2-eq emissions for each fleet type. In the case of F-CB, the total CO_2-eq emission is calculated by multiplying the amount of CO_2-eq emission per kilometer (in kg/km)[4] by the total traveled distance (in km). For the drones, we have multiplied the total energy consumption (in kWh) by the amount of carbon dioxide generated during the electricity production (in kg/kWh)[5] Finally, for the E-CBs, the total CO_2-eq emission is obtained as the product of the traveled distance, the amount of carbon dioxide generated during the electricity production, and the E-CB energy consumption per kilometer (in kWh/km).[6]

The results show that E-CBs are the most eco-friendly vehicles. In fact, drones and F-CBs generate 0.19 and 3.04 kg of CO_2-eq emissions more than the E-CBs (about 1.72 and 7.23 times more than E-CBs). These results are also consistent with the findings of Rodrigues et al. (2022) who showed the E-CBs contribution to the CO_2-eq emission is considerably lower than other vehicle types, including drones.

Last but not least, we have compared different fleet settings in terms of annual vehicle cost. Following the work of Fraselle et al. (2021), we express the annual cost in terms of a *kilometer term*, an *hourly term*, and a *daily term* (data adopted from Fraselle et al. (2021)). The kilometer term (in €/km) includes all the expenses related to the fuel/electricity usage, tyres and the maintenance and repair. The kilometer term is multiplied by the annual average distance traveled by the vehicle. The hourly term (in €/h) expresses

[3] https://earth.google.com.

[4] https://www.co2everything.com/co2e-of/motorbike.

[5] For Italy, in 2022, the amount of carbon dioxide due to electricity production is 0.389 kg/kWh https://www.nowtricity.com/country/italy.

[6] https://www.velove.se/news/armadillo-cargo-bike-use-6-electricity-small-electric-van.

Fig. 8. Optimal CB routes.

Fig. 9. Customers' waiting time for different fleet setting.

the salary of drivers per hour and should be multiplied by the number of working days and the daily shift duration (in hours) to obtain the contribution in the total cost. The daily term (in €/d) represents the fixed costs, including acquisition cost, insurance, and vehicle tax. They are multiplied by the number of working days to obtain the contribution in a year. The annual cost is calculated as the sum of total costs corresponding to the three terms as discussed above. Table 9 reports the total fleet cost under different fleet settings. We notice that the annual costs for drones are lower even if the fleet size is larger than that of the CBs.

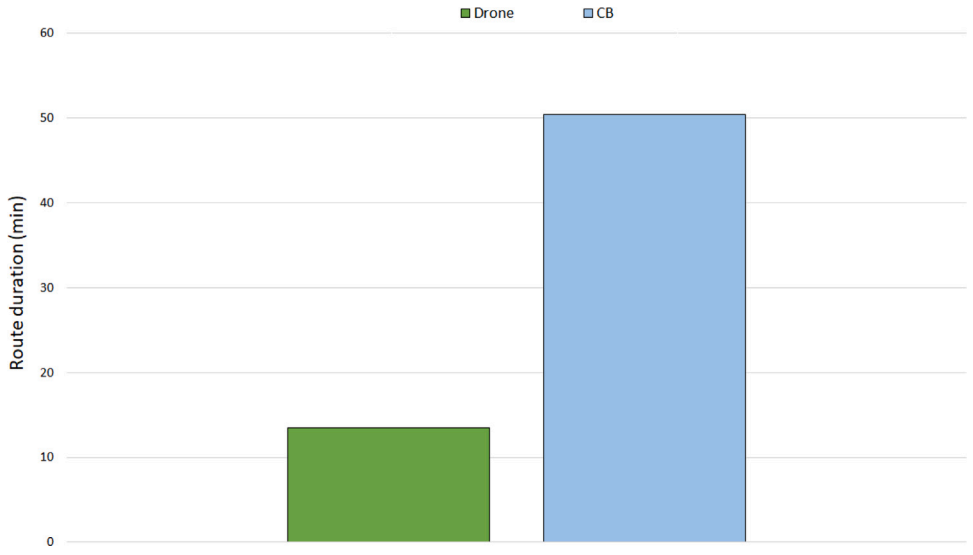

Fig. 10. Route duration under different fleet configurations.

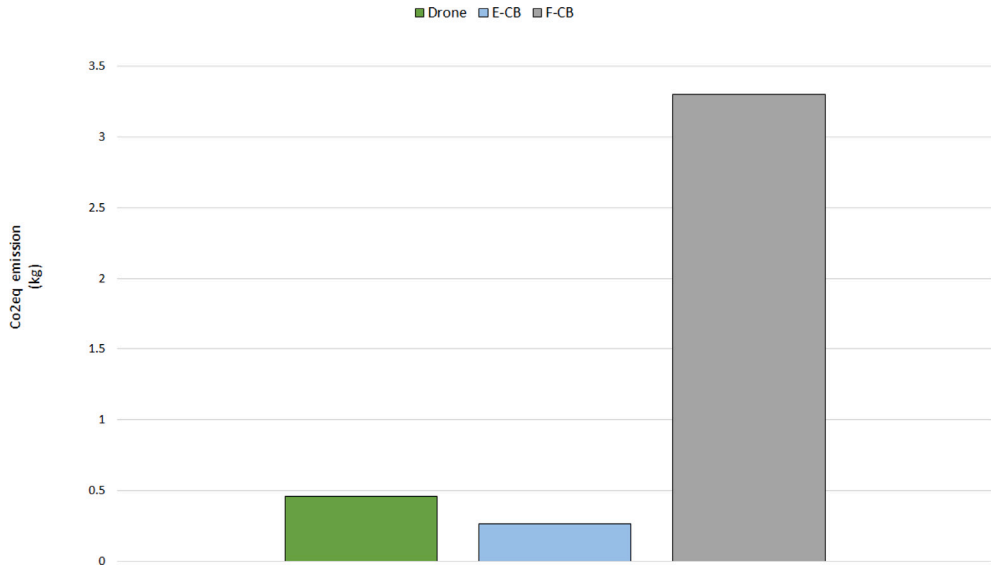

Fig. 11. Total CO_2-eq emissions under different fleet configurations.

Table 9
Total annual cost under different fleet settings.

	Drone	E-CB	F-CB
Kilometer term (€/km)	0.159	0.172	0.095
Hourly term (€/h)	11.03	19.85	22.06
Daily term (€/d)	25	2.75	4
Annual vehicle cost (€/vehicle)	23 602	34 480	34 090
Annual (fleet) cost (€)	141 612	172 400	170 450

To summarize (see Table 10), the drone-based delivery fleet shows the best performance in terms of customers' waiting time, drivers' workload, and annual cost, although E-CBs are characterized by lower CO_2-eq emissions.

Table 10
Summary of results.

	Drone	E-CB	F-CB
Waiting time (min)	6	21	21
Co_2-eq emission (kg)	0.46	0.26	3.30
Annual cost (€)	141 612	172 400	170 450

7. Conclusions

In this study, we introduced the DLLRP. This problem assumes that drones can use a set of FCs to streamline the delivery operations to a set of customers. The selection decisions and the routing plans are simultaneously optimized with the aim of minimizing the customers' waiting time. In this problem, realistic drone energy consumption functions and payload constraints were considered for drones. The uncertainty in flight times was tackled in the realm of a nonlinear robust optimization approach and deterministic counterparts were derived for two different uncertainty sets.

To cope with flight time uncertainty, which affects both the latency and energy consumption, we developed a tailored solution method, and then tested it on several instances. We also presented a real case study comparing drone-based delivery with other fleet configuration scenarios in terms of customers' waiting time, CO_2-equivalent emissions, and annual costs.

There are several fruitful directions for further research. An interesting extension of the problem considered involves the solution a drone repositioning problem. In fact, drones can be retrieved in an optimized way, to be prepared to service other customers in the next period. If the demands are known in advance for the next periods, the problem can be eventually modeled as a multi-period variant of the proposed model. In practice, the demand can only be estimated for the next period (especially considering that using drones is relevant for time-sensitive deliveries like perishable food), but it should be considered dynamic and stochastic.

CRediT authorship contribution statement

Maria Elena Bruni: Supervision, Conceptualization, Methodology, Validation, Formal analysis, Writing, Use case. **Sara Khodaparasti:** Conceptualization, Methodology, Validation, Formal analysis, Writing, Use case. **Guido Perboli:** Conceptualization, Methodology, Validation, Formal analysis, Writing, Use case.

Acknowledgment

The second author is supported by PNRR project NEST "Network 4 Energy Sustainable Transition" - PE00000021.

Appendix

The elements in the covariance matrix COV have been rounded to six digits. COV =

$$\begin{bmatrix}
0.001285 & 0.000719 & 0.001507 & 0.00098 & 0.000266 & 0.002212 & 0.00148 & 0.000189 & 0.001524 & 0.001091 & 0.000796 & 0.002755 & 0.000963 & 0.002149 & 0.001026 & 0.000597 & 0.000799 & 0.000425 & 0.00014 & 0.000603 \\
0.000719 & 0.000682 & 0.001239 & 0.000723 & 0.000158 & 0.001936 & 0.001233 & 0.000208 & 0.001462 & 0.001047 & 0.001227 & 0.002433 & 0.00104 & 0.001592 & 0.00135 & 0.000411 & 0.000767 & 0.000212 & 9.28E{-}05 & 0.001105 \\
0.001507 & 0.001239 & 0.002772 & 0.001667 & 0.000415 & 0.003221 & 0.002628 & 0.00041 & 0.003222 & 0.00229 & 0.002247 & 0.005034 & 0.002354 & 0.003103 & 0.002296 & 0.000886 & 0.001803 & 0.000509 & 0.000187 & 0.002191 \\
0.00098 & 0.000723 & 0.001667 & 0.001021 & 0.000263 & 0.001902 & 0.001576 & 0.000235 & 0.001891 & 0.001344 & 0.001222 & 0.002988 & 0.001361 & 0.001901 & 0.001264 & 0.00055 & 0.001061 & 0.000337 & 0.000117 & 0.001181 \\
0.000266 & 0.000158 & 0.000415 & 0.000263 & 7.38E{-}05 & 0.000406 & 0.000384 & 5.13E{-}05 & 0.000451 & 0.000319 & 0.000231 & 0.000708 & 0.00032 & 0.000463 & 0.000235 & 0.000142 & 0.00026 & 9.67E{-}05 & 2.98E{-}05 & 0.00023 \\
0.002212 & 0.001936 & 0.003221 & 0.001902 & 0.000406 & 0.005845 & 0.003297 & 0.000544 & 0.00368 & 0.00265 & 0.003155 & 0.006529 & 0.002492 & 0.004646 & 0.003711 & 0.001158 & 0.001838 & 0.000629 & 0.000276 & 0.002635 \\
0.00148 & 0.001233 & 0.002628 & 0.001576 & 0.000384 & 0.003297 & 0.00252 & 0.000397 & 0.003049 & 0.002171 & 0.002198 & 0.004853 & 0.002205 & 0.003061 & 0.002301 & 0.000854 & 0.001681 & 0.000486 & 0.000184 & 0.002092 \\
0.000189 & 0.000208 & 0.00041 & 0.000235 & 5.13E{-}05 & 0.000544 & 0.000397 & 6.92E{-}05 & 0.000503 & 0.000358 & 0.000422 & 0.000784 & 0.000375 & 0.000461 & 0.000433 & 0.000123 & 0.000275 & 5.8E{-}05 & 2.61E{-}05 & 0.000407 \\
0.001524 & 0.001462 & 0.003222 & 0.001891 & 0.000451 & 0.00368 & 0.003049 & 0.000503 & 0.003872 & 0.002751 & 0.002915 & 0.005907 & 0.002897 & 0.003437 & 0.002901 & 0.000974 & 0.002177 & 0.000509 & 0.0002 & 0.0029 \\
0.001091 & 0.001047 & 0.00229 & 0.001344 & 0.000319 & 0.00265 & 0.002171 & 0.000358 & 0.002751 & 0.001955 & 0.002081 & 0.004209 & 0.002055 & 0.00246 & 0.002079 & 0.000694 & 0.001543 & 0.000363 & 0.000143 & 0.002062 \\
0.000796 & 0.001227 & 0.002247 & 0.001222 & 0.000231 & 0.003155 & 0.002198 & 0.000422 & 0.002915 & 0.002081 & 0.002777 & 0.004453 & 0.002239 & 0.002434 & 0.002805 & 0.00062 & 0.001582 & 0.000214 & 0.000128 & 0.002708 \\
0.002755 & 0.002433 & 0.005034 & 0.002988 & 0.000708 & 0.006529 & 0.004853 & 0.000784 & 0.005907 & 0.004209 & 0.004453 & 0.009409 & 0.00429 & 0.005887 & 0.004668 & 0.001619 & 0.003236 & 0.000887 & 0.000349 & 0.004225 \\
0.000963 & 0.00104 & 0.002354 & 0.001361 & 0.00032 & 0.002492 & 0.002205 & 0.000375 & 0.002897 & 0.002055 & 0.002239 & 0.00429 & 0.002216 & 0.002345 & 0.002155 & 0.000674 & 0.001651 & 0.000328 & 0.000133 & 0.002289 \\
0.002149 & 0.001592 & 0.003103 & 0.001901 & 0.000463 & 0.004646 & 0.003061 & 0.000461 & 0.003437 & 0.00246 & 0.002434 & 0.005887 & 0.002345 & 0.004139 & 0.002796 & 0.001112 & 0.00181 & 0.000679 & 0.000255 & 0.002105 \\
0.001026 & 0.00135 & 0.002296 & 0.001264 & 0.000235 & 0.003711 & 0.002301 & 0.000433 & 0.002901 & 0.002079 & 0.002805 & 0.004668 & 0.002155 & 0.002796 & 0.002976 & 0.000689 & 0.00152 & 0.000268 & 0.000152 & 0.00261 \\
0.000597 & 0.000411 & 0.000886 & 0.00055 & 0.000142 & 0.001158 & 0.000854 & 0.000123 & 0.000974 & 0.000694 & 0.00062 & 0.001619 & 0.000674 & 0.001112 & 0.000689 & 0.000312 & 0.00053 & 0.000199 & 6.94E{-}05 & 0.000559 \\
0.000799 & 0.000767 & 0.001803 & 0.001061 & 0.00026 & 0.001838 & 0.001681 & 0.000275 & 0.002177 & 0.001543 & 0.001582 & 0.003236 & 0.001651 & 0.00181 & 0.00152 & 0.00053 & 0.001247 & 0.000279 & 0.000105 & 0.001622 \\
0.000425 & 0.000212 & 0.000509 & 0.000337 & 9.67E{-}05 & 0.000629 & 0.000486 & 5.8E{-}05 & 0.000509 & 0.000363 & 0.000214 & 0.000887 & 0.000328 & 0.000679 & 0.000268 & 0.000199 & 0.000279 & 0.000148 & 4.52E{-}05 & 0.000172 \\
0.00014 & 9.28E{-}05 & 0.000187 & 0.000117 & 2.98E{-}05 & 0.000276 & 0.000184 & 2.61E{-}05 & 0.0002 & 0.000143 & 0.000128 & 0.000349 & 0.000133 & 0.000255 & 0.000152 & 6.94E{-}05 & 0.000105 & 4.52E{-}05 & 1.6E{-}05 & 0.000107 \\
0.000603 & 0.001105 & 0.002191 & 0.001181 & 0.00023 & 0.002635 & 0.002092 & 0.000407 & 0.0029 & 0.002062 & 0.002708 & 0.004225 & 0.002289 & 0.002105 & 0.00261 & 0.000559 & 0.001622 & 0.000172 & 0.000107 & 0.002749
\end{bmatrix}$$

References

Balas, E., Jeroslow, R., 1972. Canonical cuts on the unit hypercube. SIAM J. Appl. Math. 23 (1), 61–69.

Barmpounakis, E., Geroliminis, N., 2020. On the new era of urban traffic monitoring with massive drone data: The pNEUMA large-scale field experiment. Transp. Res. C 111, 50–71.

Beck, J.C., 2010. Checking-up on branch-and-check. In: Cohen, D. (Ed.), Principles and Practice of Constraint Programming – CP 2010. Springer Berlin Heidelberg, Berlin, Heidelberg, pp. 84–98.

Ben-Tal, A., Den Hertog, D., Vial, J.-P., 2015. Deriving robust counterparts of nonlinear uncertain inequalities. Math. Program. 149 (1), 265–299.

Ben-Tal, A., Nemirovski, A., 2002. Robust optimization – methodology and applications. Math. Program. 92 (3), 453–480. http://dx.doi.org/10.1007/s101070100286.

Benarbia, T., Kyamakya, K., 2022. A literature review of drone-based package delivery logistics systems and their implementation feasibility. Sustainability 14 (1).

Bensinger, G., 2013. Amazon's drones for deliveries. Wall Str. J. https://www.wsj.com/articles/BL-DGB-31148, Last accessed: 06/07/2023.

Beraldi, P., Bruni, M.E., Laganà, D., Musmanno, R., 2019. The risk-averse traveling repairman problem with profits. Soft Comput. 23 (9), 2979–2993.

Bruni, M., Beraldi, P., Khodaparasti, S., 2018. A fast heuristic for routing in post-disaster humanitarian relief logistics. Transp. Res. Procedia 30, 304–313. http://dx.doi.org/10.1016/j.trpro.2018.09.033, EURO Mini Conference on "Advances in Freight Transportation and Logistics".

Bruni, M., Beraldi, P., Khodaparasti, S., 2020a. A hybrid reactive GRASP heuristic for the risk-averse k-traveling repairman problem with profits. Comput. Oper. Res. 115, 104854. http://dx.doi.org/10.1016/j.cor.2019.104854.

Bruni, M.E., Beraldi, P., Khodaparasti, S., 2020d. A hybrid reactive GRASP heuristic for the risk-averse k-traveling repairman problem with profits. Comput. Oper. Res. 115, 104854.

Bruni, M.E., Khodaparasti, S., 2022. A variable neighborhood descent matheuristic for the drone routing problem with beehives sharing. Sustainability 14 (16).

Bruni, M., Khodaparasti, S., Beraldi, P., 2020b. The selective minimum latency problem under travel time variability: An application to post-disaster assessment operations. Omega 92, 102154. http://dx.doi.org/10.1016/j.omega.2019.102154.

Bruni, M., Khodaparasti, S., Beraldi, P., 2020c. The selective minimum latency problem under travel time variability: An application to post-disaster assessment operations. Omega 92, 102154.

Bruni, M.E., Khodaparasti, S., Demeulemeester, E., 2020e. The distributionally robust machine scheduling problem with job selection and sequence-dependent setup times. Comput. Oper. Res. 123, 105017.

Bruni, M., Khodaparasti, S., Moshref-Javadi, M., 2022. A logic-based Benders decomposition method for the multi-trip traveling repairman problem with drones. Comput. Oper. Res. 145, 105845. http://dx.doi.org/10.1016/j.cor.2022.105845.

CARS@POLITO, 2012. Center for automotive research and sustainable mobility web site. https://www.cars.polito.it/, Last accessed: 06/07/2023.

Chassein, A., Dokka, T., Goerigk, M., 2019. Algorithms and uncertainty sets for data-driven robust shortest path problems. European J. Oper. Res. 274 (2), 671–686. http://dx.doi.org/10.1016/j.ejor.2018.10.006.

Chauhan, D., Unnikrishnan, A., Figliozzi, M., 2019. Maximum coverage capacitated facility location problem with range constrained drones. Transp. Res. C 99, 1–18. http://dx.doi.org/10.1016/j.trc.2018.12.001.

Cheng, C., Adulyasak, Y., Rousseau, L.-M., 2020a. Drone routing with energy function: Formulation and exact algorithm. Transp. Res. B 139, 364–387.

Cheng, C., Adulyasak, Y., Rousseau, L.-M., Sim, M., 2020b. Robust Drone Delivery with Weather Information. Optimization-online.org, URL http://www.optimization-online.org/DB_HTML/2020/07/7897.html.

Chowdhury, S., Emelogu, A., Marufuzzaman, M., Nurre, S.G., Bian, L., 2017. Drones for disaster response and relief operations: A continuous approximation model. Int. J. Prod. Econ. 188, 167–184. http://dx.doi.org/10.1016/j.ijpe.2017.03.024.

Crainic, t., Perboli, G., Ricciardi, N., 2021. City logistics. In: Crainic, t., Gendreau, M., Gendron, B. (Eds.), Network Design with Applications in Transportation and Logistics. Springer, Boston, pp. 507–537, (chapter 16).

Di Puglia Pugliese, L., Guerriero, F., Scutellá, M.G., 2021. The last-mile delivery process with trucks and drones under uncertain energy consumption. J. Optim. Theory Appl. 191 (1), 31–67.

Dorling, K., Heinrichs, J., Messier, G.G., Magierowski, S., 2016. Vehicle routing problems for drone delivery. IEEE Trans. Syst. Man Cybern.: Syst. 47 (1), 70–85.

Dukkanci, O., Kara, B.Y., Bektaş, T., 2021. Minimizing energy and cost in range-limited drone deliveries with speed optimization. Transp. Res. C 125, 102985. http://dx.doi.org/10.1016/j.trc.2021.102985.

Evers, L., Dollevoet, T., Barros, A.I., Monsuur, H., 2014. Robust UAV mission planning. Ann. Oper. Res. 222 (1), 293–315. http://dx.doi.org/10.1007/s10479-012-1261-8.

Fraselle, J., Limbourg, S.L., Vidal, L., 2021. Cost and environmental impacts of a mixed fleet of vehicles. Sustainability 13 (16), 9413.

Geromel Dotto, H., Thor Magnusson, K., 2022. Total cost of ownership optimization model for battery-electric trucks.

Ghelichi, Z., Gentili, M., Mirchandani, P.B., 2021. Logistics for a fleet of drones for medical item delivery: A case study for Louisville, KY. Comput. Oper. Res. 135, 105443. http://dx.doi.org/10.1016/j.cor.2021.105443.

Golabi, M., Shavarani, S.M., Izbirak, G., 2017. An edge-based stochastic facility location problem in UAV-supported humanitarian relief logistics: a case study of tehran earthquake. Nat. Hazards 87 (3), 1545–1565.

Goodchild, A., Toy, J., 2018. Delivery by drone: An evaluation of unmanned aerial vehicle technology in reducing CO2 emissions in the delivery service industry. Transp. Res. D 61, 58–67.

Grogan, S., Pellerin, R., Gamache, M., 2021. Using tornado-related weather data to route unmanned aerial vehicles to locate damage and victims. OR Spectrum 43 (4), 905–939.

Huang, Y., Zhao, L., Van Woensel, T., Gross, J.-P., 2017. Time-dependent vehicle routing problem with path flexibility. Transp. Res. B 95, 169–195.

Kanellos, M., 2014. Forbes. Google working on drones too. https://www.forbes.com/sites/michaelkanellos/2014/08/29/google-working-on-drones-too/?sh=1d0c93ce79a7, Last accessed: 06/07/2023.

Kim, S., Kwak, J.H., Oh, B., Lee, D.-H., Lee, D., 2021. An optimal routing algorithm for unmanned aerial vehicles. Sensors 21 (4), 1219.

Kim, S.J., Lim, G.J., Cho, J., 2018. Drone flight scheduling under uncertainty on battery duration and air temperature. Comput. Ind. Eng. 117, 291–302.

Kim, S.J., Lim, G.J., Cho, J., Côté, M.J., 2017. Drone-aided healthcare services for patients with chronic diseases in rural areas. J. Intell. Robot. Syst. 88 (1), 163–180.

Kolvenbach, P., Lass, O., Ulbrich, S., 2018. An approach for robust PDE-constrained optimization with application to shape optimization of electrical engines and of dynamic elastic structures under uncertainty. Opt. Eng. 19, 697–731.

Kronqvist, J., Bernal, D.E., Lundell, A., Grossmann, I.E., 2019. A review and comparison of solvers for convex MINLP. Opt. Eng. 20 (2), 397–455.

Kyriakakis, N.A., Marinaki, M., Matsatsinis, N., Marinakis, Y., 2022. A cumulative unmanned aerial vehicle routing problem approach for humanitarian coverage path planning. European J. Oper. Res. 300 (3), 992–1004. http://dx.doi.org/10.1016/j.ejor.2021.09.008.

Li, X., Li, P., Zhao, Y., Zhang, L., Dong, Y., 2021. A hybrid large neighborhood search algorithm for solving the multi depot UAV swarm routing problem. IEEE Access 9, 104115–104126.

Liu, Y., Liu, Z., Shi, J., Wu, G., Chen, C., 2019. Optimization of base location and patrol routes for unmanned aerial vehicles in border intelligence, surveillance, and reconnaissance. J. Adv. Transp. 2019.

Macias, J.E., Angeloudis, P., Ochieng, W., 2020. Optimal hub selection for rapid medical deliveries using unmanned aerial vehicles. Transp. Res. C 110, 56–80.
Macrina, G., Di Puglia Pugliese, L., Guerriero, F., Laporte, G., 2020. Drone-aided routing: A literature review. Transp. Res. C 120, 102762. http://dx.doi.org/10.1016/j.trc.2020.102762.
Matl, P., Hartl, R.F., Vidal, T., 2018. Workload equity in vehicle routing problems: A survey and analysis. Transp. Sci. 52 (2), 239–260.
McKinsey, 2023. Drones take to the sky, potentially disrupting last-mile delivery. https://www.mckinsey.com/industries/aerospace-and-defense/our-insights/future-air-mobility-blog/drones-take-to-the-sky-potentially-disrupting-last-mile-delivery, Last accessed: 06/07/2023.
Melkonyan, A., Gruchmann, T., Lohmar, F., Kamath, V., Spinler, S., 2020. Sustainability assessment of last-mile logistics and distribution strategies: The case of local food networks. Int. J. Prod. Econ. 228, 107746. http://dx.doi.org/10.1016/j.ijpe.2020.107746.
Mittal, S., et al., 2011. Algorithms for Discrete, Non-Linear and Robust Optimization Problems with Applications in Scheduling and Service Operations (Ph.D. thesis). Massachusetts Institute of Technology.
Moshref-Javadi, M., Winkenbach, M., 2021. Applications and research avenues for drone-based models in logistics: A classification and review. Expert Syst. Appl. 177, 114854.
Nucamendi-Guillén, S., Martínez-Salazar, I., Angel-Bello, F., Moreno-Vega, J.M., 2016. A mixed integer formulation and an efficient metaheuristic procedure for the k-travelling repairmen problem. J. Oper. Res. Soc. 67 (8), 1121–1134.
Nucamendi-Guillén, S., Martínez-Salazar, I., Khodaparasti, S., Bruni, M.E., 2022. New formulations and solution approaches for the latency location routing problem. Comput. Oper. Res. 143, 105767. http://dx.doi.org/10.1016/j.cor.2022.105767.
Panadero, J., Juan, A.A., Bayliss, C., Currie, C., 2020. Maximising reward from a team of surveillance drones: a simheuristic approach to the stochastic team orienteering problem. Eur. J. Ind. Eng. 14 (4), 485–516.
Perboli, G., Brotcorne, L., Bruni, M.E., Rosano, M., 2021a. A new model for last-mile delivery and satellite depots management: The impact of the on-demand economy. Transp. Res. E 145, 102–184.
Perboli, G., Rosano, M., 2019. Parcel delivery in urban areas: Opportunities and threats for the mix of traditional and green business models. Transp. Res. C 99, 19–36. http://dx.doi.org/10.1016/j.trc.2019.01.006.
Perboli, G., Rosano, M., Saint-Guillain, M., Rizzo, P., 2018a. Simulation-optimisation framework for city logistics: an application on multimodal last-mile delivery. IET Intell. Transp. Syst. 12 (4), 262–269. http://dx.doi.org/10.1049/iet-its.2017.0357.
Perboli, G., Rosano, M., Saint-Guillain, M., Rizzo, P., 2018b. A simulation-optimization framework for city logistics. An application on multimodal last-mile delivery. IET Intell. Transp. Syst. 12 (4), 262–269.
Perboli, G., Rosano, M., Wei, Q., 2021b. A simulation-optimization approach for the management of the on-demand parcel delivery in sharing economy. IEEE Trans. Intell. Transp. Syst..
Poikonen, S., Campbell, J.F., 2021. Future directions in drone routing research. Networks 77 (1), 116–126.
Pulver, A., Wei, R., 2018. Optimizing the spatial location of medical drones. Appl. Geogr. 90, 9–16.
Radzki, G., Bocewicz, G., Golińska-Dawson, P., Jasiulewicz-Kaczmarek, M., Witczak, M., Banaszak, Z., 2021a. Periodic planning of uavs' fleet mission with the uncertainty of travel parameters. In: 2021 IEEE International Conference on Fuzzy Systems (FUZZ-IEEE). IEEE, pp. 1–8.
Radzki, G., Golinska-Dawson, P., Bocewicz, G., Banaszak, Z., 2021b. Modelling robust delivery scenarios for a fleet of unmanned aerial vehicles in disaster relief missions. J. Intell. Robot. Syst. 103 (4), 63. http://dx.doi.org/10.1007/s10846-021-01502-2.
Rodrigues, T.A., Patrikar, J., Oliveira, N.L., Matthews, H.S., Scherer, S., Samaras, C., 2022. Drone flight data reveal energy and greenhouse gas emissions savings for very small package delivery. Patterns 3 (8), 100569.
Thibbotuwawa, A., Bocewicz, G., Radzki, G., Nielsen, P., Banaszak, Z., 2020. UAV mission planning resistant to weather uncertainty. Sensors 20 (2), 515.
Thorsteinsson, E., 2001. Branch-and-check: A hybrid framework integrating mixed integer programming and constraint logic programming. In: Proceedings of the International Conference on Principles and Practice of Constraint Programming, Vol. 2239. pp. 16–30. http://dx.doi.org/10.1007/3-540-45578-7_2,
Torabbeigi, M., Lim, G.J., Kim, S.J., 2020. Drone delivery scheduling optimization considering payload-induced battery consumption rates. J. Intell. Robot. Syst. 97 (3), 471–487.
Troudi, A., Addouche, S.-A., Dellagi, S., Mhamedi, A.E., 2018. Sizing of the drone delivery fleet considering energy autonomy. Sustainability 10 (9), 3344.
Ulmer, M.W., Thomas, B.W., 2018. Same-day delivery with heterogeneous fleets of drones and vehicles. Networks 72 (4), 475–505.
Verge, T., 2023. Alphabet's Wing is working on larger drones that can handle heavier deliveries. https://www.theverge.com/2022/7/14/23217294/wing-drone-delivery-package-size-prototype, Last accessed: 06/07/2023.
Vural, D., Dell, R.F., Kose, E., 2021a. Locating unmanned aircraft systems for multiple missions under different weather conditions. Oper. Res. 21 (1), 725–744. http://dx.doi.org/10.1007/s12351-019-00455-7.
Vural, D., Dell, R.F., Kose, E., 2021b. Locating unmanned aircraft systems for multiple missions under different weather conditions. Oper. Res. 21 (1), 725–744.
Wei, Q., 2022. Last-Mile Logistics Optimization in the On-Demand Economy (Ph.D. thesis). Politecnico di Torino 2022.
Yakıcı, E., 2016. Solving location and routing problem for UAVs. Comput. Ind. Eng. 102, 294–301.
Yuan, Y., Li, Z., Huang, B., 2018. Nonlinear robust optimization for process design. AIChE J. 64 (2), 481–494.
Zhang, J., Campbell, J.F., Sweeney II, D.C., Hupman, A.C., 2021. Energy consumption models for delivery drones: A comparison and assessment. Transp. Res. D 90, 102668.
Zhang, G., Jia, N., Zhu, N., Adulyasak, Y., Ma, S., 2023. Robust drone selective routing in humanitarian transportation network assessment. European J. Oper. Res. 305 (1), 400–428. http://dx.doi.org/10.1016/j.ejor.2022.05.046.
Zhang, J., Li, Y., 2023. Collaborative vehicle-drone distribution network optimization for perishable products in the epidemic situation. Comput. Oper. Res. 149, 106039. http://dx.doi.org/10.1016/j.cor.2022.106039.
Zhu, T., Boyles, S.D., Unnikrishnan, A., 2022. Two-stage robust facility location problem with drones. Transp. Res. C 137, 103563. http://dx.doi.org/10.1016/j.trc.2022.103563.
Zipline, 2023. Zipline expands United States operations and adds new customers in the food, retail and transportation sectors. https://www.flyzipline.com/articles/zipline-expands-united-states-operations-and-adds-new-customers-in-the-food-retail-and-transportation-sectors, Last accessed: 06/07/2023.